JOURNAL OF GEOPHYSICAL RESEARCH, VOL. 108, NO. C8, 3281, doi:10.1029/2002JC001417, 2003

***Correction published 16 February 2007***

# Dynamics of mean and subtidal flow on the New England shelf

R. Kipp Shearman and Steven J. Lentz

Department of Physical Oceanography, Woods Hole Oceanographic Institution, Woods Hole, Massachusetts, USA

Received 27 March 2002; revised 7 March 2003; accepted 10 April 2003; published 29 August 2003.

[1] Current and hydrographic observations from the Coastal Mixing and Optics experiment moored array, deployed from August 1996 through June 1997, are used to describe the velocity variability and evaluate the dynamics of circulation over the New England shelf on timescales ranging from a few days to several months. Subtidal (days to weeks) current variability was polarized along-isobath and dominated by episodic bursts of westward flow. The along-isobath subtidal flow was primarily geostrophic and barotropic, and was correlated with large-scale along-coast wind stress fluctuations oriented 45°T (65° counterclockwise from the local isobath orientation). Subtidal near-surface ageostrophic transport matched estimates of wind-driven Ekman transport; however, near-bottom ageostrophic transport was much larger than estimates of Ekman transport from bottom stress. Low-frequency (monthly and longer timescales) flow was generally westward and off-shelf at all sites and depths, with the strongest westward flow during the fall. Low-frequency along-isobath currents were primarily geostrophic with baroclinic and barotropic components of similar magnitude. Depth-averaged ageostrophic transport was quantitatively consistent with Ekman transport from wind and bottom stress. Measured bottom stress at both subtidal and low-frequency timescales was weak, nearly an order of magnitude smaller than the wind stress. Low-frequency fluctuations in the predominantly geostrophic along-isobath flow were attributable to variations in the cross-shelf density field associated with the seasonal cycle in surface heating. During the fall, thermal wind shear was strongest, because the cross-isobath temperature gradient was acting in concert with the persistent cross-isobath salinity gradient to enhance the cross-isobath density gradient (i.e., warmer and fresher water inshore). During the winter, in response to surface cooling, the cross-isobath temperature gradient reversed sign, reducing the cross-isobath density gradient (i.e., cooler and fresher water inshore). *INDEX TERMS:* 4219 Oceanography: General: Continental shelf processes; 4572 Oceanography: Physical: Upper ocean processes; 4512 Oceanography: Physical: Currents; *KEYWORDS:* coastal oceanography, dynamics, wind-driven circulation, shelf-slope front, Middle Atlantic Bight

**Citation:** Shearman, R. K., and S. J. Lentz, Dynamics of mean and subtidal flow on the New England shelf, *J. Geophys. Res.*, *108*(C8), 3281, doi:10.1029/2002JC001417, 2003.

## 1. Introduction

[2] A densely instrumented moored array was deployed on the New England shelf south of Cape Cod (Figure 1) as part of the Office of Naval Research sponsored Coastal Mixing and Optics (CMO) experiment [*Dickey and Williams*, 2001]. The CMO moored array was deployed from August 1996 through June 1997, spanning the seasonal breakdown of stratification in the fall and rebuilding of stratification in the spring [*Lentz et al.*, 2003], and was instrumented to measure oceanic variables (velocity, temperature, conductivity, bottom pressure, and near-bottom stress) with high vertical resolution, as well as along- and cross-isobath resolution, and the atmospheric forcing (wind stress, surface heat, and buoyancy flux). These observations are used here to characterize the flow over the New England shelf on timescales ranging from a few days to several months. In addition, the concomitant high-quality observations of bottom pressure, wind stress, bottom stress, and density (from conductivity and temperature) throughout the water column provide the opportunity to examine the dynamics of the flow over the New England shelf. The CMO moored observations are the only long (spanning the seasonal stratification cycle) time series of conductivity throughout the water column with both along- and cross-isobath resolution on the New England shelf. This is important because the structure of the density field potentially plays a critical role in the dynamics of shelf circulation [e.g., *Chapman and Lentz*, 1994], and temperature alone is insufficient to characterize the density field.

[3] The first objective of this work is to describe the variability of currents on the New England shelf over subtidal (ST; approximately 2–15 days) and low-frequency


0148-0227/03/2002JC001417$09.00

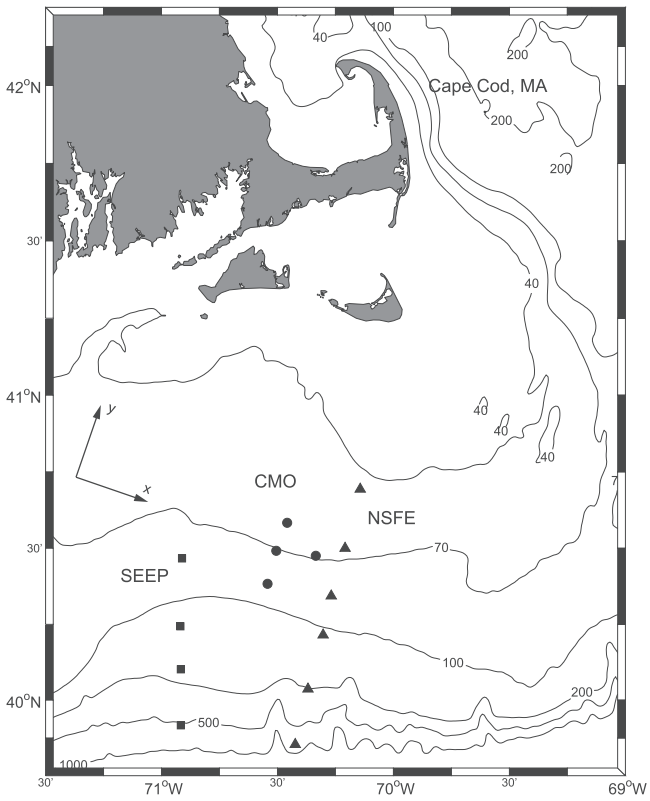


**Figure 1.** CMO experiment site and bathymetry. Locations of the CMO mooring sites are indicated by a dot. Also shown are the sites of previous moored observations from SEEP (squares) and NSFE (triangles).

(LF; approximately 1–10 months) timescales. The second objective is to provide an interpretation of the associated dynamics: quantifying the relative importance of geostrophic and ageostrophic flow, characterizing the vertical structure (e.g., barotropic versus baroclinic effects), and evaluating the important physical processes affecting the circulation (i.e., wind-forcing, stratification, and density fronts). The remainder of this paper is organized as follows: section 2 describes the CMO field program and the observations made from the moored array; section 3 presents an overview of circulation on the New England shelf, based on previous observations and the CMO observations of wind stress, density and current variability; sections 4 and 5 examine the mean currents and LF current variability in terms of their geostrophic and ageostrophic components; section 6 examines the ST current variability in terms of its relationship to wind stress variability, as well as its geostrophic and ageostrophic components; section 7 discusses some physical processes affecting LF and ST current variability; and section 8 summarizes the preceding material.

## 2. CMO Moored Array and Analysis Methods

[4] The CMO moored array consisted of four sites located approximately 100 km south of Cape Cod (Figure 1), occupied continuously from August 1996 through June 1997. The densely instrumented central site was located at 40° 29.5′N, 70° 30.5′W in 70 m of water. Three surrounding sites were located approximately 11 km inshore in 64 m of water, 12.5 km offshore in 86 m of water, and 14.5 km east along the 70-m isobath.

[5] All four sites (central, inshore, offshore, and alongshore) included observations of currents, temperature and salinity (from conductivity), spanning the water column (Figure 2). Bottom pressure was measured at the inshore, offshore, and alongshore sites. The central site included meteorological observations from which wind stress and surface heat flux were estimated using the bulk formulas of *Fairall et al.* [1996]. Direct covariance estimates of wind stress were also made, using a sonic anemometer and motion sensor package [*Edson et al.*, 1999]. The direct covariance estimates were used to produce more accurate bulk estimates of wind stress [*Martin*, 1998]. For a shorter duration, covariance estimates of near-bottom stress were made from velocimeters mounted on a bottom tripod [*Shaw et al.*, 2001] at the central site (see below).

[6] A thorough description of the moored instrumentation, sampling strategies, and data processing techniques is contained in the data report by *Galbraith et al.* [1999]. Additional details for temperature, conductivity, and surface meteorological observations are provided by *Lentz et al.* [2003]. Bottom pressure was sampled every 5 min using Seagauge pressure sensors (SBE 26), mounted to the anchors, at the inshore, offshore, and alongshore sites. Currents were observed using 25 vector-measuring current meters

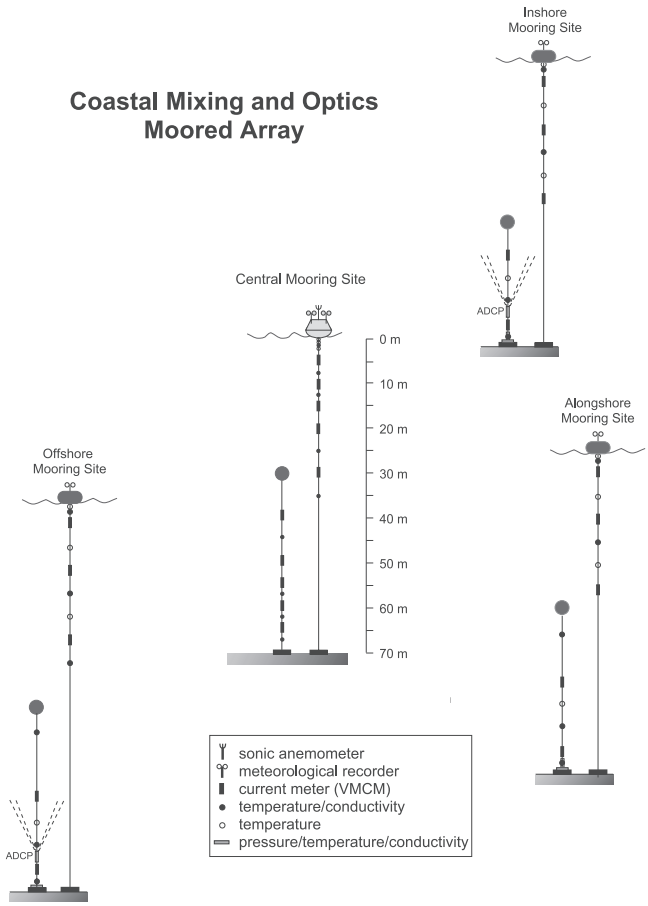


**Figure 2.** Schematic drawing of CMO mooring array.

**Table 1.** Statistics of Depth-Averaged Currents and Local Isobath Orientation

| Site | Mean cm $s^{-1}$ | Direction, °T | Major Axis, cm $s^{-1}$ | Minor Axis, cm $s^{-1}$ | Orientation, °T | Isobath Orientation, °T |
|---|---|---|---|---|---|---|
| Inshore | 5.2 | 271 | 9.9 | 3.4 | 116 | 119 |
| Central | 7.6 | 270 | 10.8 | 3.4 | 112 | 112 |
| Offshore | 8.3 | 269 | 10.9 | 3.7 | 118 | 106 |

(VMCMs) and, for a shorter period (August to December 1996), two upward-looking 300 kHz RD Instruments acoustic Doppler current profilers (ADCPs). The sample interval for VMCMs was 7.5 min and for ADCPs was 3 min. Typical rms differences between ADCP and VMCM observations at the same depth were less than 3 cm $s^{-1}$, and regression slopes were between 0.85 and 1.05 with correlations greater than 0.95. Raw observation time series were low-pass filtered (1 hour cut-off) and decimated to hourly values. To remove variability due to tidal, inertial, and higher-frequency fluctuations, the hourly time series were low-pass filtered (33 hour cut-off). The accuracy of an hourly estimate was approximately 2–3 cm $s^{-1}$ for current [*Beardsley*, 1987], 0.05°C for temperature, and 0.1 for salinity (pss).

### 2.1. Along/Cross-Isobath Coordinates

[7] A coordinate system for the subsequent analysis was determined by the orientation of the principal axes of the depth-averaged subtidal current meter observations (Table 1). The depth-averaged currents were computed via

$$\langle \mathbf{u} \rangle = \frac{1}{H} \int_{-H}^{0} \mathbf{u} dz, \tag{1}$$

where $H$ is the water depth at each site, $\mathbf{u} = (u, v)$ is the horizontal velocity vector, and the integration is performed assuming that $\mathbf{u}$ is constant between the surface (bottom) and topmost (deepest) observation.

[8] The orientation of the depth-averaged, subtidal principal axes is within 3° of the orientation of the local isobaths (Table 1), determined from a high-resolution Gulf of Maine bathymetry data set compiled by the United States Geological Survey (Figure 1). The positive $x$-axis (along-isobath direction) is oriented 110°T, and the positive $y$-axis (cross-isobath direction) is oriented 20°T. The orientation of both the depth-averaged, subtidal principal axes and local isobaths varies in the cross-shelf direction. However, changes of ±5° in the coordinate system orientation do not qualitatively affect the results presented below.

### 2.2. Bottom Stress

[9] At the central site, near-bottom currents and direct covariance estimates of near-bottom stress were made from acoustic travel-time velocimeters mounted on a bottom tripod [*Williams et al.*, 1987], the Benthic Acoustic Stress Sensor (BASS). The BASS tripod recorded currents and near-bottom stress at 7 depths; 63.0, 64.6, 66.7, 67.8, 68.9, 69.3, and 69.6 m in 70 m of water. Three BASS deployments over the course of the CMO experiment returned useful data; 18 August to 27 September 96, 7 October to 16 November 1996, and 17 April to10 June 1997. For this analysis, we use the stress estimate at 69.3 m to represent bottom stress. A quadratic drag law was then used to relate the deepest central site current meter observation (59.5 m) to hourly estimates of bottom stress;

$$\boldsymbol{\tau}^b = \rho_0 C_d \mathbf{u}^\mathbf{b} \left| \mathbf{u}^\mathbf{b} \right|, \tag{2}$$

where $\rho_0$ = 1025 kg $m^{-3}$ is the time/volume-averaged density, and $C_d$ is the dimensionless drag coefficient. The drag coefficient that produced the best agreement (determined by linear regression) was $C_d = (0.51 \pm 0.02) \times 10^{-3}$ for both components with a correlation of 0.85 (0.77) for the along-isobath (cross-isobath) component. The quadratic drag law was used to fill gaps (mainly in winter) in the direct covariance estimates of bottom stress over the duration of the CMO experiment.

### 2.3. Calculation of Geostrophic and Ageostrophic Currents

[10] Absolute geostrophic currents are estimated from the moored observations of density and bottom pressure. The pressure at $z$ = 0 m ($P^0$) is computed from bottom pressure and density, assuming the flow is hydrostatic [e.g., *Brown et al.*, 1985],

$$P^0 = P^b - \int_{-H}^{0} g\rho dz, \tag{3}$$

where $P^b$ is the bottom pressure and $g$ = 9.81 m $s^{-2}$ is the gravitational acceleration. Pressure at depth $z$ is $P(z) = P^0 + B(z)$, where

$$B = \int_{z}^{0} g\rho dZ. \tag{4}$$

The barotropic (BT) and baroclinic (BC) components of the geostrophic currents are computed, using equations (3) and (4) and the geostrophic relation,

$$(u^g_{\mathrm{BT}}, v^g_{\mathrm{BT}}) = \frac{1}{\rho_0 f} \left( -\frac{\partial P^0}{\partial y}, \frac{\partial P^0}{\partial x} \right), \tag{5}$$

$$\left(u^g_{\mathrm{BC}}, v^g_{\mathrm{BC}}\right) = \frac{1}{\rho_0 f} \left( -\frac{\partial B}{\partial y}, \frac{\partial B}{\partial x} \right) \tag{6}$$

where $f = 9.44 \times 10^{-5}$ $s^{-1}$ is the local Coriolis parameter. Absolute geostrophic velocity ($\mathbf{u}^g$) is the sum of equations (5) and (6). Because of very low frequency drifts in the observations of bottom pressure, estimates of absolute geostrophic velocity are highly uncertain on timescales longer than about 2 months. Thermal wind shear is directly estimated from the density observations as

$$\frac{\partial \mathbf{u}^g}{\partial z} = \frac{g}{\rho_0 f} \left( \frac{\partial \rho}{\partial y}, -\frac{\partial \rho}{\partial x} \right). \tag{7}$$

Further details regarding the calculation of geostrophic currents (i.e., estimation of density and pressure gradients) are contained in Appendix A. Observed currents ($\mathbf{u}^{obs}$) are spatially averaged over the scale of the pressure gradients, following *Brown et al.* [1985], when compared to geostrophic currents (see Appendix A). Ageostrophic currents are computed as the difference between the observed and absolute geostrophic currents ($\mathbf{u}^{ag} = \mathbf{u}^{obs} - \mathbf{u}^{g}$).

## 3. Overview of Circulation on the New England Shelf

[11] The dominant physical characteristics of New England shelf water are the marked seasonal change in temperature and the presence of the shelf-slope front. During the summer, New England shelf water is thermally stratified with a strong thermocline at about 20 m [*Bigelow*, 1933; *Beardsley et al.*, 1985; *Linder and Gawarkiewicz*, 1998]. Below the thermocline, water temperatures reach a minimum over the middle to outer shelf; this band of cold water that is continuous along most of the Middle Atlantic Bight (MAB) is called the "cold pool" [*Houghton et al.*, 1982]. In the fall, thermal stratification is removed by cooling and increased mixing by winter storms. *Lentz et al.* [2003] have shown that stratification is primarily removed by large downwelling-favorable wind events. Thermal stratification then rebuilds in the spring. In general, the broad cross-shelf structure of temperature and salinity are low (cool and fresh) at the coast and increase in the offshore direction. In the summertime, though, temperature has a mid-shelf minimum due to the cold pool. The shelf-slope front is a region of sharp gradients separating the relatively cool, fresh shelf water and warm, salty slope water [*Islen*, 1936; *Houghton et al.*, 1988; *Linder and Gawarkiewicz*, 1998]. The foot of the shelf-slope front is typically located near the 100-m isobath on the New England shelf [*Linder and Gawarkiewicz*, 1998], and may undergo cross-isobath displacements of 10–20 km due to upwelling- or downwelling-favorable winds [*Houghton et al.*, 1988; *Lentz et al.*, 2003].

[12] During CMO, stratification on the shelf undergoes a large seasonal change (Figure 3b) that is qualitatively similar to previous descriptions. Beginning in August, shelf water was strongly stratified. Stratification decreased during the fall, until a state of near-zero stratification was achieved in December. Throughout the rest of the winter, the shelf water generally remained stratified at the moored array, due to the anomalous on-shelf location of the foot of the shelf-slope front [*Lentz et al.*, 2003]. During the spring, stratification redeveloped, due to surface heating, augmented by an intrusion of anomalously fresh water from the Connecticut River [*Lentz et al.*, 2003].

[13] Previous moored observations in the vicinity of the CMO experiment site (Figure 1) include the 1979–1980 Nantucket Shoals Flux Experiment (NSFE) [*Beardsley et al.*, 1985] and the 1983–1984 Shelf Edge Exchange Processes (SEEP-1) study [*Aikman et al.*, 1988]. Mean flow for both studies was along-shelf toward the west between 5 and 10 cm $s^{-1}$. Shelf currents from NSFE and SEEP did not exhibit a significant seasonal variation, but there were seasonal differences in the wind-driven response. In summer, current variations were moderately correlated with wind stress, while in winter, wind and currents were highly correlated, but the response (amount of current per unit wind stress) was larger during the summer.

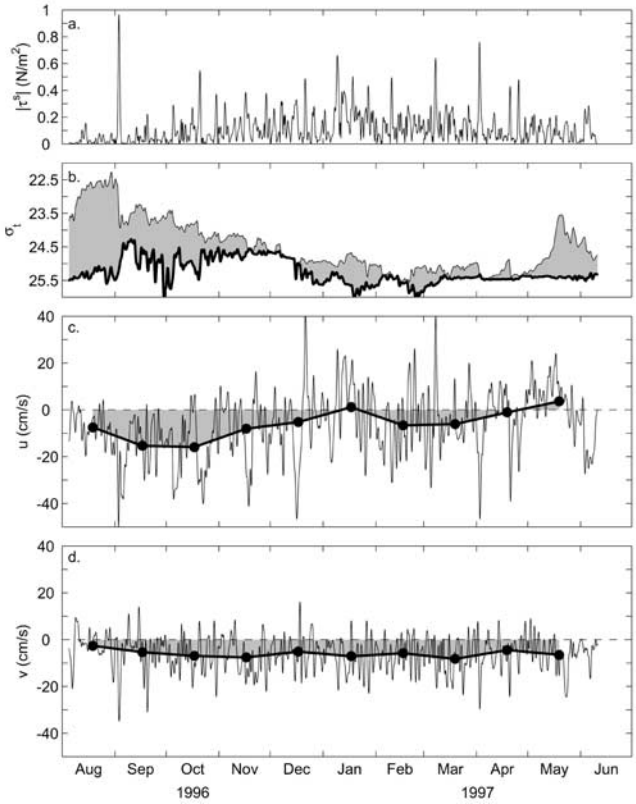


**Figure 3.** Low-pass filtered (33 hour cut-off) time series from the moored observations of (a) wind stress magnitude (N $m^{-2}$), (b) near-surface (7.5 m, thin line) and near-bottom (68.1 m, thick line) density, (c) along-isobath current at 4.6 m with monthly average (thick shaded line), and (d) cross-isobath current at 4.6 m with monthly average (thick shaded line). All observations are from the central site.

[14] During CMO, the filtered wind stress observations are punctuated by several intense events, lasting 1–3 days (Figure 3a). These events were typically associated with storms passing near the CMO site. The strong wind stress event in early September 1996 (Figure 3a) was hurricane Edouard [*Chang and Dickey*, 2001]. The maximum wind stress magnitude, associated with passing storms, approached 1.0 N $m^{-2}$ during hurricane Edouard, and otherwise ranged from 0.3 to 0.7 N $m^{-2}$. Wind stress variability was dominated by these isolated, episodic events during the fall (August through December) and spring (April though June). During the winter, wind stress was more continuous rather than episodic. During the fall and spring, strong wind stress events were followed by strong along-isobath currents persisting for 7–10 days (Figure 3c). These episodic current events were predominantly westward. During the winter, along-isobath currents were less episodic, with eastward and westward flow occurring equally. Cross-isobath currents were smaller than along-isobath flow, and at monthly timescales were consistently off-shelf (Figure 3d).

[15] From previous observation and modeling studies, wind stress forcing is recognized as a primary source of

subtidal current and sea level variability over the New England shelf [*Wang*, 1979; *Ou et al.*, 1981; *Noble et al.*, 1983; *Beardsley et al.*, 1985; *Wright et al.*, 1986; *Greenberg et al.*, 1997]. Both local and remote (e.g., due to coastal trapped waves (CTWs)) forcing contribute to current variability, but previous research has shown that on the New England shelf the local wind-forced response dominates [*Wang*, 1979; *Ou et al.*, 1981]. The subtidal wind-driven response is thought to be largely barotropic and geostrophic. However, this is somewhat conjectural since the corresponding observations of vertical structure and density gradients were not made in the past. Furthermore, variations in the structure of the density field, such as the seasonal cycle of stratification, may yield variations in the wind-driven current response.

[16] Because the mean flow is generally opposed to the mean wind stress, low-frequency currents on the New England and MAB shelf are thought to be driven by an along-shelf pressure gradient [e.g., *Stommel and Leetma*, 1972; *Csanady*, 1976]. Dynamically, an along-shelf pressure gradient is required to maintain the mean geostrophic flow against a bottom drag that is usually assumed to be linearly related to the mean flow. There are potentially different sources for an along-shelf pressure gradient along the MAB, but the most likely seems to be the upstream input of fresh water [*Beardsley and Winant*, 1979]. This along-shelf pressure gradient driving implies that low-frequency flow variations are the result of changes in the upstream condition (fresh water flux) that travel down to the New England shelf, rather than local changes. The along-shelf pressure gradient required to drive a 5–10 cm $s^{-1}$ along-shelf flow is small and has not yet been observed. Models of mean flow on the New England shelf often assume a strong barotropic component [e.g., *Chapman et al.*, 1986], or conclude that baroclinic effects, such as thermal wind shear from cross-shelf density gradients, are negligible [e.g., *Stommel and Leetma*, 1972]. These assumptions assure a strong (equivalent to the depth-average) near-bottom flow that generates drag. An alternate scenario for mean flow is a highly baroclinic vertical structure (i.e., thermal wind) that results in small near-bottom currents and weak bottom stress [e.g., *Garrett et al.*, 1993]. This case has not been previously explored, mainly because there have been no long-term observations of bottom stress or density gradients over the New England shelf.

[17] The following sections will examine current variability during CMO on timescales related to the low-frequency (mean to monthly) and the subtidal (episodic wind stress events) variability. The examination will focus on the dynamics of the flow, looking at the geostrophic and ageostrophic components and their relation to wind forcing and seasonal changes over the shelf.

## 4. Mean Currents

[18] The full record (10 month) mean currents, for the CMO experiment, are westward and off-shelf at all sites and depths (Figure 4). Mean currents range from 3 to 11 cm $s^{-1}$, with along-isobath currents larger than cross-isobath currents, except near the surface, where both are nearly equal in magnitude. Mean wind stress is small, about 0.035 N $m^{-2}$

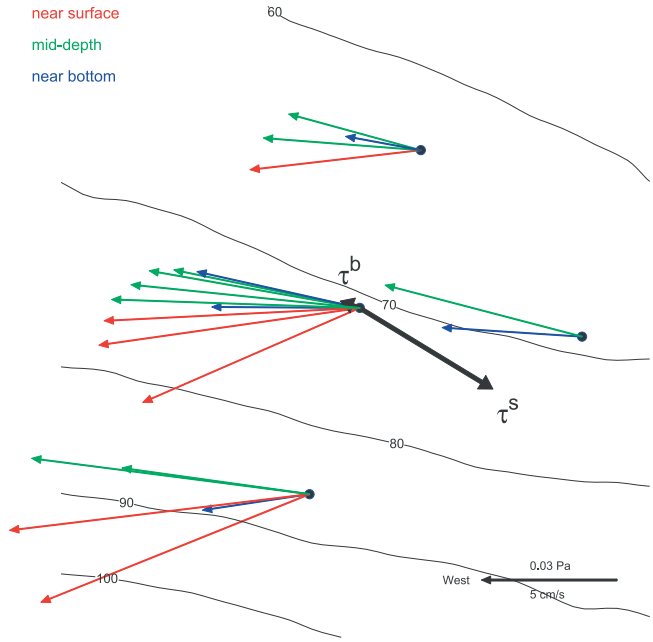


**Figure 4.** Full record mean wind stress, bottom stress, and currents. The 60-, 70-, 80-, 90-, and 100-m isobaths are shown. Color indicates depth: surface to 15 m, red; 20 mab to bottom, blue; mid-depth, green.

(Figure 4), and directed eastward, opposite the mean currents. Mean bottom stress is a factor of 7 smaller than the mean wind stress, about 0.005 N $m^{-2}$, and oriented along-isobath to the west.

[19] The vertical structure of the mean currents is similar at all sites. Mean currents are oriented most strongly off-shelf near the surface, and turn clockwise (CW) with depth between the surface and about 20 mab (meters-above-bottom), where mean currents are aligned most closely with the local isobaths (Figure 4). Below 20 mab, the mean currents turn counterclockwise (CCW) with depth. Along-isobath currents have a mid-depth maximum between 15 and 30 m. Cross-isobath currents are largest near the surface, decrease to a minimum at 20 mab, and increase slightly toward the bottom (Figure 5). Mean current at the surface is inferred via linear extrapolation. Also, the near-bottom tripod current observations span a shorter time period than the central site VMCM observations. However, computing the VMCM mean currents from the common time period does not qualitatively change the results.

[20] Mean cross-isobath currents above 30 m increase slightly in the off-shelf direction, while below 30 m, there is no discernible cross-shelf variation. Mean along-isobath currents increase in the off-shelf direction at all depths. For example, mean along-isobath currents at 30 m depth increase from −5.6 cm $s^{-1}$ (inshore) to −10.1 cm $s^{-1}$ (offshore), and the resulting mean cross-isobath shear is $0.02f$. This suggests that mean nonlinear terms in the momentum balances (i.e., $vu_y$) are small relative to the Coriolis term (i.e., $fv$), but this persistent shear may significantly influence other current variability such as near-inertial oscillations [e.g., *Kunze*, 1985], and will be examined in future research.

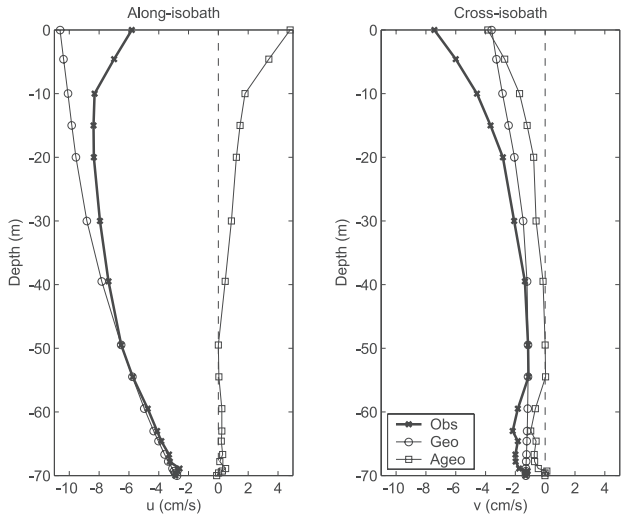


**Figure 5.** Profiles of the mean observed, geostrophic, and ageostrophic (a) along-isobath and (b) cross-isobath currents.

[21] Owing to the uncertainties in the very low frequency variability of the bottom pressure observations (see Appendix A), estimates of the mean BT geostrophic currents are unreliable. The mean BC geostrophic currents, however, are determined with more certainty, since they depend only on the observations of density. The mean BT geostrophic currents are inferred by assuming the observed mean flow is geostrophic ($\mathbf{u}^g = \mathbf{u}^{obs}$) at $z$ = 50 m (20 mab). The resulting mean BT geostrophic currents are $-10.6$ cm s$^{-1}$ (along-isobath) and $-3.6$ cm s$^{-1}$ (cross-isobath).

[22] Mean geostrophic currents are westward and off-shelf at all depths (Figure 5), with mean along-isobath geostrophic flow much larger than mean cross-isobath flow. Both mean along- and cross-isobath geostrophic currents are strongest near the surface, and geostrophic shear increases toward the bottom for along-isobath flow, while geostrophic shear weakens toward the bottom for cross-isobath flow. There is a mean depth-averaged cross-isobath geostrophic flow of $-1.8$ cm s$^{-1}$, which is about half of the total observed depth-averaged cross-isobath flow.

[23] Mean ageostrophic flow is eastward and off-shelf at all depths (Figure 5). Both components of mean ageostrophic flow are similar in magnitude, except near the bottom, where cross-isobath ageostrophic flow is larger than along-isobath flow. Mean ageostrophic currents are strongest near the surface, decrease to a minimum at 20 mab (zero by definition), and have a local maximum at about 8 mab. The mean ageostrophic currents are consistent in direction with Ekman transport from mean wind and bottom stresses (Figure 4). Mean Ekman transport (scaled by depth),

$$\langle \mathbf{u}_{\mathrm{EK}} \rangle = \left(\tau^{sy} - \tau^{by}, \tau^{bx} - \tau^{sx}\right)/\rho_0 fH, \qquad (8)$$

is $(-0.10,-0.54)$ cm s$^{-1}$, while depth-averaged ageostrophic flow is $(1.00,-0.84)$ cm s$^{-1}$. However, if mean values are computed for only the time period with BASS tripod observations, then the Ekman and ageostrophic transports are $(-0.10,-0.31)$ cm s$^{-1}$ and $(1.16,-0.33)$ cm s$^{-1}$. Mean cross-isobath Ekman and ageostrophic transports are nearly equal, while along-isobath transports are not, which may be due to errors in the inferred BT geostrophic flow or estimates of cross-isobath density gradients, a distinct possibility given the resolution of the CMO array (23 km) and the characteristic length scales (about 10 km) associated with the shelf-slope front [*Linder and Gawarkiewicz*, 1998].

## 5. Low-Frequency Currents

[24] Seasonal mean currents are computed for the fall (04 August 1996 to 1 December 1996), winter (1 December 1996 to 1 April 1997) and spring (1 April 1997 to 14 June 1997). Definitions for fall, winter, and spring arise from the seasonal variations in surface heat flux, wind stress, and stratification [see *Lentz et al.*, 2003]. Seasonal mean currents are westward and off-shelf at all sites and depths (Figure 6), with a vertical structure nearly identical to the full record means. Like the full record mean currents, seasonal mean along-isobath currents also increase in the off-shelf direction. The principal seasonal variation is in the magnitude of the along-isobath flow, which is largest in the fall and smallest in the spring (almost zero near the surface). Seasonal mean cross-isobath currents are slightly stronger near the surface in the winter. Seasonal mean wind stress is larger during the winter and weaker during the fall and spring (Table 2). Mean bottom stress is larger during the fall than winter or spring, but nearly an order of magnitude smaller than seasonal mean wind stresses.

[25] To avoid uncertainty in the very low frequency estimates of the BT pressure gradients, we will compare monthly mean estimates of thermal wind shear to monthly mean observed shear to evaluate geostrophy (Figure 7). The correspondence between the observed and geostrophic along-isobath shear is weak near the surface (0–20 m), and strong at mid-depths (20–50 m) and near the bottom (20–0 mab). Mid-depth and near-bottom geostrophic shears are very similar to observed, with correlations of 0.70 and

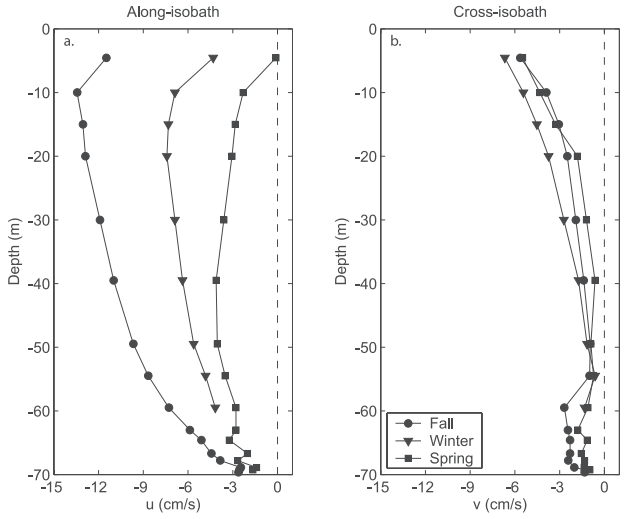


**Figure 6.** Profiles of the fall, winter, and spring mean (a) along-isobath and (b) cross-isobath currents at the central site.

**Table 2.** Statistics of Subtidal Wind and Bottom Stress for the Full Record and the Fall, Winter, and Spring Periods

| | Mean, N m$^{-2}$ | Direction, °T | Major Axis, N m$^{-2}$ | Minor Axis, N m$^{-2}$ | Orientation °T |
|---|---|---|---|---|---|
| | | | *Wind Stress* | | |
| Full record | 0.03 | 121 | 0.11 | 0.11 | 85 |
| Fall | 0.02 | 161 | 0.11 | 0.08 | 172 |
| Winter | 0.06 | 109 | 0.15 | 0.12 | 90 |
| Spring | 0.02 | 110 | 0.10 | 0.07 | 21 |
| | | | *Bottom Stress* | | |
| Full record | 0.005 | 290 | 0.017 | 0.006 | 94 |
| Fall | 0.006 | 283 | 0.015 | 0.007 | 89 |
| Winter | 0.003 | 305 | 0.019 | 0.006 | 99 |
| Spring | 0.004 | 287 | 0.015 | 0.003 | 91 |

0.80 (99% confidence level is 0.75) and linear regression slopes of 1.0 ± 0.9 and 0.9 ± 0.6, respectively. Observed and geostrophic cross-isobath shears are uncorrelated at mid-depths and only weakly correlated near the surface (0.12) and bottom (0.17).

[26] Monthly averages of Ekman transport from (8) are similar to monthly mean depth-averaged ageostrophic flow (Figure 8), with the BT geostrophic component inferred as before. Monthly mean depth-averaged cross-isobath ageostrophic flow is correlated (0.80) with the cross-isobath Ekman transport, and the transport values are similar (offset of 0.2 cm s$^{-1}$ and linear regression slope of 1.1 ± 0.6). The least agreement between cross-isobath Ekman and ageostrophic transport occurs during the fall. Monthly mean depth-averaged along-isobath ageostrophic transport is correlated (0.89) with the along-isobath Ekman transport with a linear regression slope of 0.7 ± 0.3, but the transport values are offset by a larger amount (−0.6 cm s$^{-1}$). Like the full record mean ageostrophic transport, monthly mean depth-averaged ageostrophic currents are small compared to the total geostrophic currents, and uncertainties in estimating the mean BT geostrophic currents (particularly the along-isobath currents) and cross-shelf density gradients could substantially influence the estimates of ageostrophic transport.

## 6. Subtidal Current Variability

[27] Standard deviations of the subtidal (ST) currents are about 11 and 4 cm s$^{-1}$ for the along- and cross-isobath components, respectively (Figure 9). Subtidal current variability is polarized in the along-isobath direction at all sites and depths, with ellipticities (ratio of the minor to major axes) that range from 0.3 to 0.6, and orientations that are within 15° of the local isobath orientation. Polarization of the ST currents is weaker near the surface, and strongest at approximately 20 mab. Subtidal standard deviations for both the along- and cross-isobath currents are strongest near the surface, and relatively constant between 20 m and 20 mab. Within 20 m of the bottom, standard deviation of the along-isobath currents decrease, while cross-isobath currents are roughly constant to within 2–3 m of the bottom. The subtidal standard deviation of the along-isobath flow at all depths and cross-isobath flow above 30 m increases slightly in the off-shelf direction.

[28] The vertical and horizontal structure of ST standard deviations, during the fall, winter, and spring, are similar to the full record vertical structure. Subtidal along-isobath current variability is strongest during the winter and weakest during the spring (Figure 9). In the upper half of the water column, ST cross-isobath current variability is strongest during the fall, and in the lower half, cross-isobath current variability is strongest during the winter. Subtidal standard deviations of cross-isobath currents are weakest during the spring.

[29] Wind stress variability is not polarized in any particular direction during CMO, with equal major and minor principal axes of 0.11 N m$^{-2}$ (Table 2). Wind stress

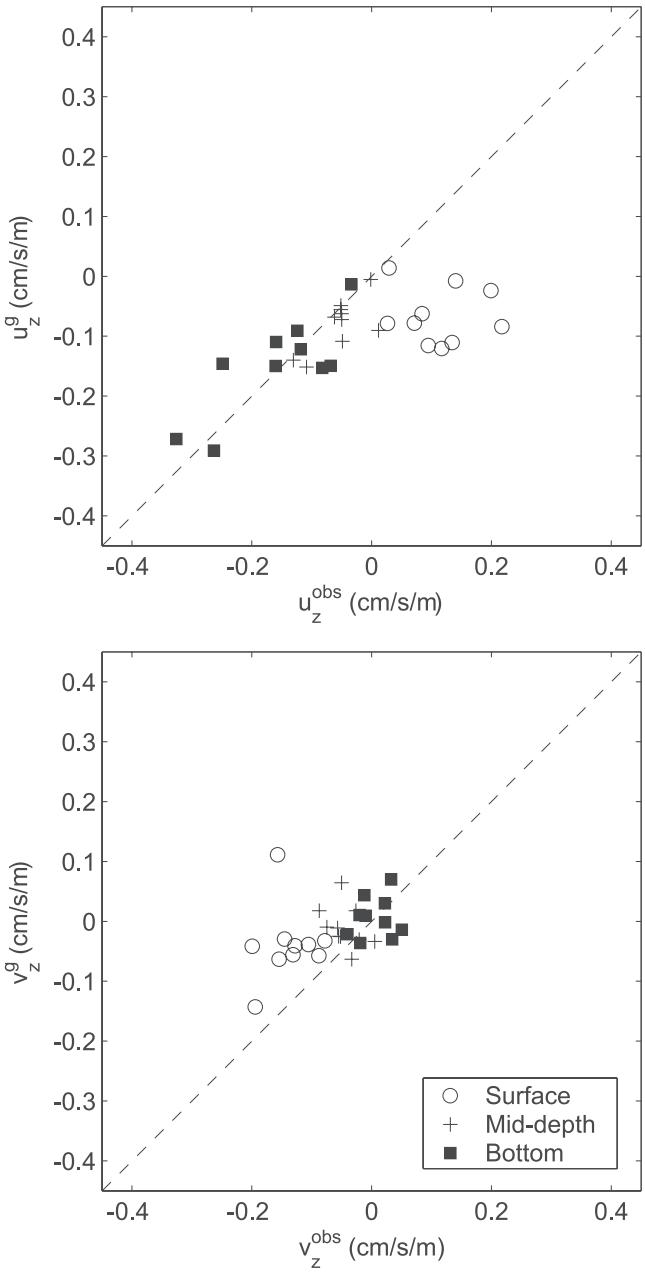


**Figure 7.** Comparison of observed and geostrophic monthly mean (a) along-isobath and (b) cross-isobath shear. Shear estimates are averages over the depth ranges 0–20 m (near surface), 20–50 m (mid-depth), and 50–70 m (20–0 mab, near bottom).

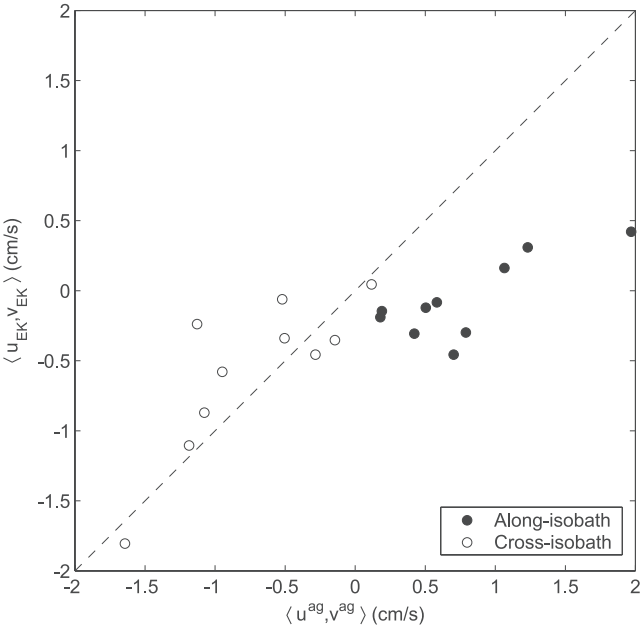


**Figure 8.** Monthly mean depth-averaged ageostrophic currents compared to monthly mean Ekman transport from equation (8). Along-isobath (cross-isobath) currents are indicated by solid (open) symbols.

variability is strongest during the winter and weakest in spring. Subtidal bottom stress variability is nearly an order of magnitude less than the wind stress variability (Table 2), and is polarized in approximately the along-isobath direction. Seasonally, along-isobath bottom stress variability is largest in winter and weakest in spring.

[30] The depth-averaged, along-isobath, ST current variability is correlated most strongly with the wind stress component oriented approximately 45°T (65° CCW from the local isobath orientation), and lagged the wind stress by about 11 hours (Table 3). The maximum correlation between wind stress and depth-averaged along-isobath currents increased in the onshore direction, while the angle and lag were nearly constant. Seasonally, the maximum correlation between depth-averaged along-isobath currents and wind stress was always significant (largest during winter), and orientation and lag were generally the same as the full record values, except for two discrepancies: lag at the central and alongshore sites during the fall (discussed below) and wind stress orientation at the inshore, central, and offshore sites during the spring.

[31] Depth-averaged cross-isobath currents were significantly correlated with ST wind stress, with maximum correlation values ranging from 0.48 to 0.60. The maximum correlation between wind stress and depth-averaged cross-isobath currents did not have a distinct cross-isobath structure. Maximum correlation values between the wind stress and the depth-averaged cross-isobath currents did not vary substantially over the fall, winter, and spring periods. Orientation angles and time-lag values varied substantially, but there was no coherent seasonal signal to either orientation angle or lag. In all seasons, the orientation of the wind stress component that had maximum correlation with depth-averaged cross-isobath currents increased (became more north-south oriented) in the offshore direction, while lag decreased.

[32] At the central and alongshore sites, lags for maximum correlation between depth-averaged along-isobath flow and wind stress oriented 45°T are much longer than the typical 9–12 hours seen during the winter and spring. The reason for the apparent discrepancy is related to the shape of the wind-current correlation function and its dependence on season and cross-shelf location. During the fall and spring, the wind-current correlation function has a broad peak, encompassing time lags from 10 to 50 hours, while during the winter the peak is narrow and centered on about 11 hours (Figure 10). At the central and offshore sites, during the fall, there are local maxima at lags of about 11 and 44 hours. The increased correlation between the wind stress and along-isobath currents at time lags of approximately 40 hours during the fall (and broader peak in spring) is due to the duration of the current response to the (largely downwelling-favorable) episodic wind events. During the

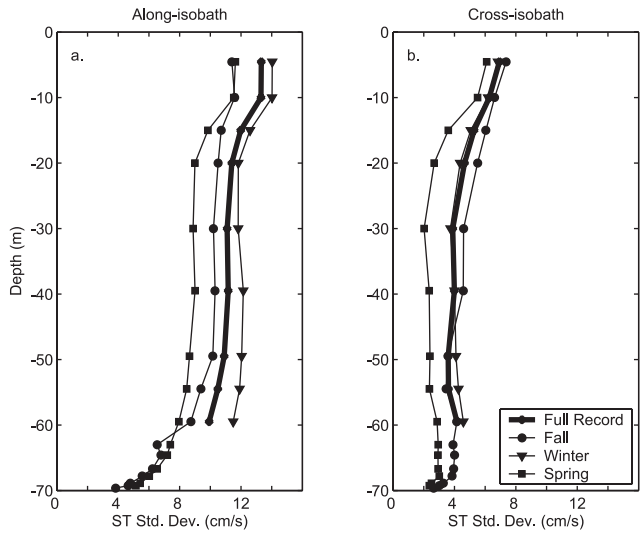


**Figure 9.** Profiles of the standard deviation of the ST (a) along-isobath and (b) cross-isobath currents at the central site, computed over the full record, fall, winter, and spring periods.

**Table 3.** Maximum Correlation for a Given Lag (in Hours) Between the ST Wind Stress Component Oriented in Direction θ (°T) and the Depth-Averaged Along- and Cross-Isobath Currents, Computed Over the Full Record, Fall, Winter, and Spring Period[a]

| | Full Record | | | Fall | | | Winter | | | Spring | | |
|---|---|---|---|---|---|---|---|---|---|---|---|---|
| | Cor | θ | Lag | Cor | θ | Lag | Cor | θ | Lag | Cor | θ | Lag |
| $\langle u_i \rangle$ | 0.73 | 45 | 10 | 0.61 | 48 | 12 | 0.81 | 48 | 9 | 0.77 | 15 | 10 |
| $\langle u_c \rangle$ | 0.69 | 47 | 10 | 0.50 | 54 | 44 | 0.81 | 47 | 10 | 0.77 | 28 | 11 |
| $\langle u_o \rangle$ | 0.61 | 45 | 11 | 0.41 | 46 | 12 | 0.74 | 45 | 11 | 0.72 | 35 | 11 |
| $\langle u_a \rangle$ | 0.63 | 54 | 12 | 0.54 | 46 | 39 | 0.86 | 47 | 12 | ... | ... | ... |
| $\langle v_i \rangle$ | 0.56 | 300 | 12 | 0.54 | 312 | 8 | 0.60 | 290 | 15 | 0.47 | 290 | 17 |
| $\langle v_c \rangle$ | 0.60 | 329 | 8 | 0.55 | 325 | 8 | 0.66 | 333 | 8 | 0.56 | 321 | 6 |
| $\langle v_o \rangle$ | 0.48 | 355 | 6 | 0.40 | 332 | 8 | 0.57 | 6 | 4 | 0.66 | 346 | 8 |
| $\langle v_a \rangle$ | 0.52 | 324 | 6 | 0.54 | 327 | 6 | 0.68 | 59 | 146 | ... | ... | ... |

[a]Correlations greater than 0.25 (full record), 0.35 (fall and winter), and 0.50 (spring) are significant at the 95% confidence level, using a decorrelation timescale of 100 hours for the ST currents.

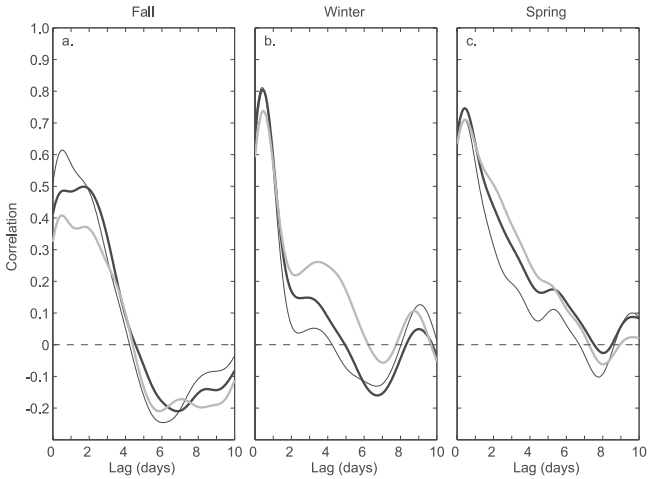


**Figure 10.** Time-lagged correlation between the wind stress component oriented toward 45°T and the depth-averaged along-isobath currents at the inshore (thin black line), central (thick black line), and offshore (thick shaded line) sites for the (a) fall, (b) winter, and (c) spring periods.

fall and spring, the along-isobath currents persist for 7–10 days after large downwelling-favorable wind stress events (see Figure 3). During the winter, there are fewer episodic downwelling events like the fall and spring, and wind stress forcing changes direction from upwelling to downwelling favorable more often. Rapid changes in wind direction may potentially prevent the slower (40-hour lag) wind-driven response from happening. Also, the difference in wind-driven current response may be associated with stronger stratification [*Beardsley et al.*, 1985], because during CMO, fall and spring periods are more stratified near the surface than winter.

[33] The correlation and lag relationships between wind stress and along-isobath currents are consistent with the process of wind-driven coastal setup/setdown and propagating coastal trapped waves [e.g., *Schwing*, 1992a, 1992b]. However, the response over the New England shelf is dominated by local forcing [*Wang*, 1979]. Typically, subtidal wind-forcing on the New England shelf is the result of passing storms with large length scales transiting from southwest to northeast. The large length scales, fast propagation speed for CTWs (about 500 km $d^{-1}$), and anti-resonant propagation direction of the wind stress forcing result in a wind-driven response on the New England shelf that appears local in nature, although entirely consistent with CTW theory. Also, the orientation of the wind stress component that yields maximum correlation is not aligned with the local isobaths. This was noted, as well, by *Beardsley et al.* [1985] during NSFE. The orientation of the wind stress component was assumed to match the orientation of the large-scale coastline. We examine this assumption in the discussion. For now, we will define the wind stress component oriented 45°T as the along-coast wind stress ($\tau^{scx}$).

[34] The maximum correlation between along-coast wind stress and along-isobath currents below 30 m (Figures 11a and 11b) occurs at lags similar to the lags for the depth-

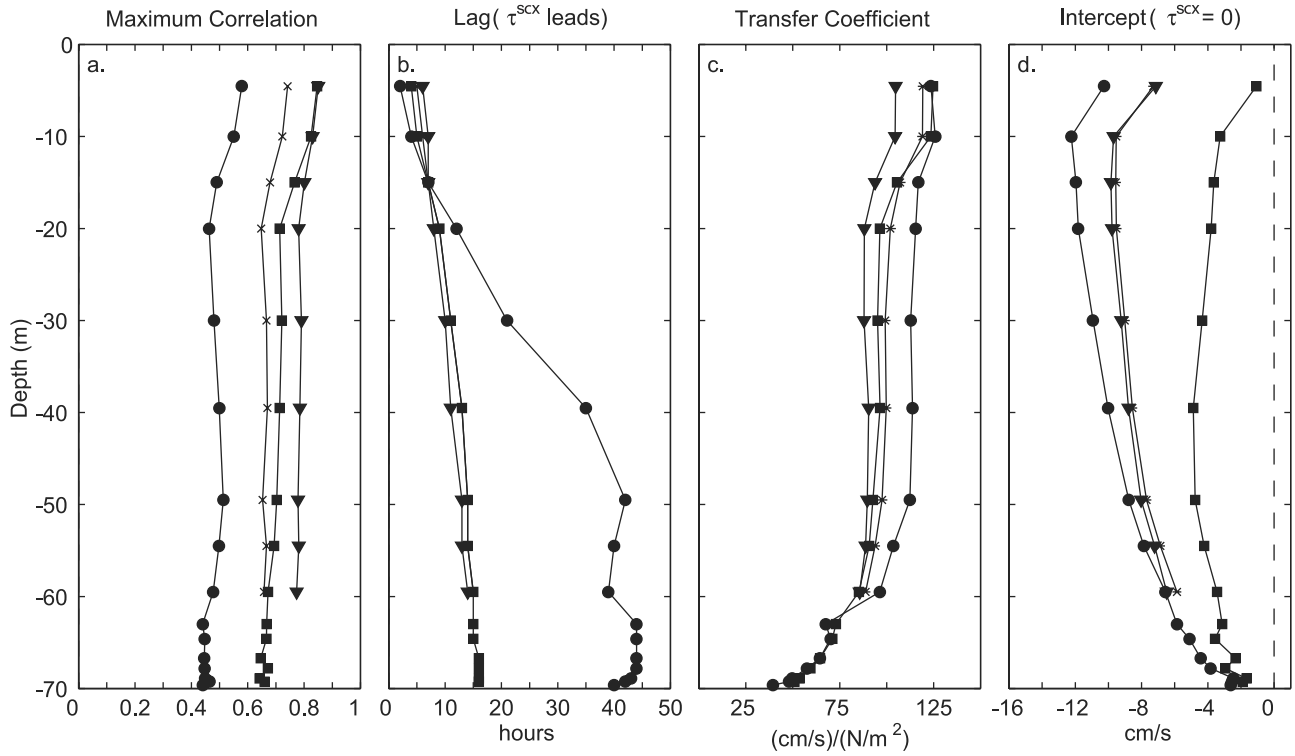


**Figure 11.** Comparison of the along-isobath currents at the central site and along-coast (45°T) wind stress: (a) maximum correlation between along-isobath current and along-coast wind stress, (b) lag (wind stress leads), (c) linear regression slopes (transfer coefficients), and (d) linear regression intercepts (flow in the absence of wind stress). Comparison is made for the full record, fall, winter, and spring periods.

averaged comparison (about 14 hours, except for fall, which is about 44 hours). Over the full record, linear regressions of the along-coast wind stress onto the lagged along-isobath currents at the central site (Figure 11c) have regression slopes (transfer coefficients) ranging from 89 ± 13 (cm $s^{-1}$)/(N $m^{-2}$) at 59.5 m to 119 ± 13 (cm $s^{-1}$)/(N $m^{-2}$) at 4.6 m. Slopes are largest above 20 m, nearly constant between 20 and 50 m, and slightly decreased below 50 m. Linear regression slopes between along-coast wind stress and along-isobath currents are smallest during the winter and largest during the fall. Above 10 m, slopes are also large during the spring. During fall and spring, when there was tripod data, regression slopes decreased from approximately 93 ± 34 (cm $s^{-1}$)/(N $m^{-2}$) at 59.5 m to 36 ± 16 (cm $s^{-1}$)/(N $m^{-2}$) at 69.6 m. Regression slopes are larger at the offshore site and smaller at the inshore site. At 30 m, the slope at the offshore site was 104 ± 22 (cm $s^{-1}$)/(N $m^{-2}$) and the slope at the inshore site is 82 ± 11 (cm $s^{-1}$)/(N $m^{-2}$).

[35] The intercepts from the linear regression of the along-coast wind stress onto the lagged along-isobath currents at the central site (Figure 11d) are remarkably similar to the observed mean along-isobath currents (Figures 5 and 6). The intercepts essentially represent the currents that persist in the absence of wind forcing (i.e., $\tau^{scx} = 0$). The significance of this fact will be discussed in section 7.

### 6.1. Subtidal Geostrophic Current Variability

[36] The ST along-isobath geostrophic current variability is dominated by the BT component (Figure 12a) with a standard deviation of 9.7 cm $s^{-1}$ versus 4.2 cm $s^{-1}$ for the largest (near-bottom) along-isobath BC geostrophic current. The cross-isobath BT and near-bottom BC geostrophic currents (Figure 12b) are nearly equal in magnitude (respective standard deviations of 4.1 and 3.6 cm $s^{-1}$) and opposite (correlation of −0.64). Baroclinic geostrophic current variability is vertically coherent. The BT geostrophic current is strongly polarized along isobath with a principal axes ellipticity of 0.4 and an orientation of

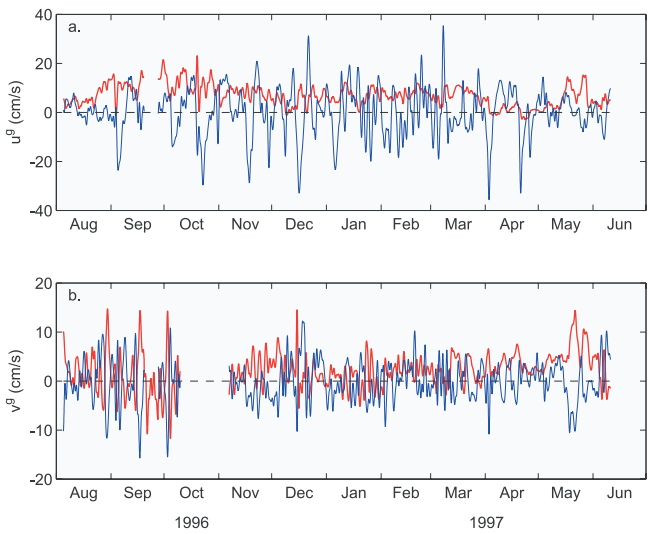


**Figure 12.** BT geostrophic velocity (blue line) and BC geostrophic velocity at 63.5 m (red line) in the (a) along-isobath and (b) cross-isobath directions.

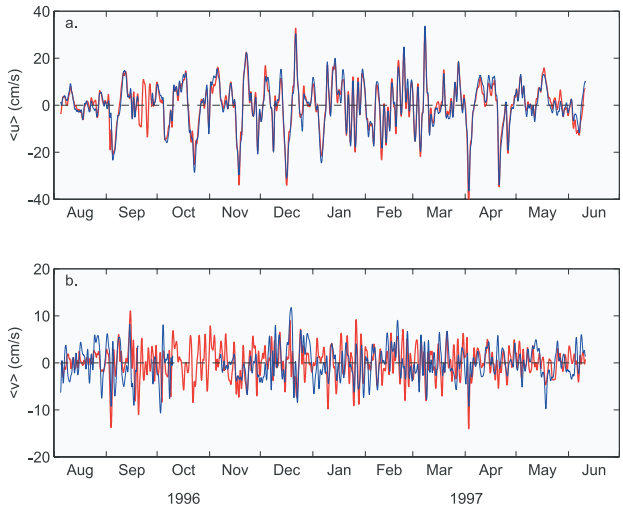


**Figure 13.** Observed (red line) and geostrophic (blue line) depth-averaged current in the (a) along-isobath and (b) cross-isobath directions.

110°T. The BC geostrophic current is not substantially polarized, with an ellipticity of 0.9 and an orientation of 111°T at 63.5 m depth. Along-isobath BT geostrophic current variability is predominately characterized by episodic bursts, having timescales of days, similar to the wind-driven events identified in the ST current meter observations (Figure 3c), while the along-isobath BC geostrophic current variability does not exhibit an episodic nature, but rather has a substantial low-frequency component, discussed in the preceding section.

[37] Previous efforts have identified the "excellent comparison" between the subtidal variability of the observed and geostrophic (estimated from bottom pressure gradient alone) along-shelf currents over the New England shelf [*Brown et al.*, 1985], and other efforts have concluded that the subtidal cross-shelf momentum balance was geostrophic, while the along-shelf momentum balance had geostrophic and ageostrophic components of similar magnitude [*Noble et al.*, 1983]. These efforts lacked density observations throughout the water column, though, and were unable to explicitly comment on the contribution of the BC component of geostrophic velocity or characterize the vertical structure of the momentum balances.

[38] The depth-averaged along-isobath flow during CMO is highly geostrophic (Figure 13a). Linear regression of the depth-averaged geostrophic along-isobath currents onto the observed yields a slope of 0.97 ± 0.03 and a correlation of 0.97. The depth-averaged geostrophic cross-isobath currents (Figure 13b) are less (but significantly) correlated to the observed currents, with a regression slope of 0.90 ± 0.21 and a correlation of 0.50.

[39] The observed and geostrophic along-isobath currents are highly correlated at all depths, ranging from 0.88 near the surface to 0.98 below 40 m (Figure 14). The linear regression slopes of the along-isobath geostrophic currents onto the observed are near 1.0 between 20 and 50 m. Near the surface, regression slopes are significantly larger than 1.0 (1.23 ± 0.08 at 4.6 m), and near the bottom, slopes are significantly smaller (0.78 ± 0.02 at 67 m). The along-

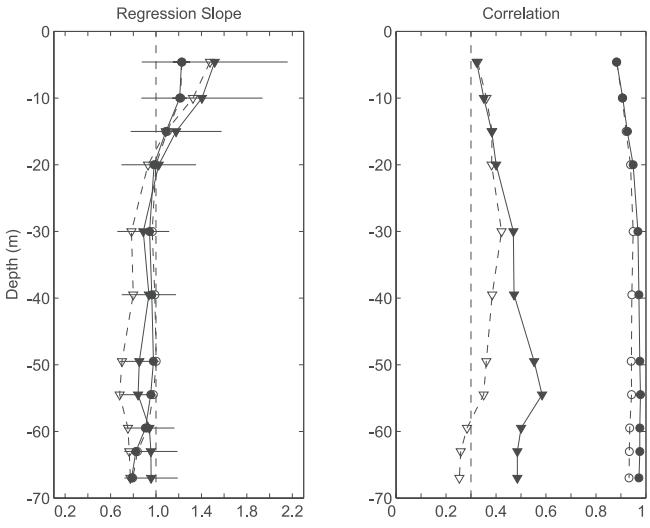


**Figure 14.** Comparison of BT (open symbols) and total (solid symbols) geostrophic currents to observed currents throughout the water column. Comparison of along-isobath currents are indicated by circles and cross-isobath currents by triangles. (a) Linear regression slopes of geostrophic current onto observed current. (b) Correlation value at zero lag.

isobath geostrophic current variability is dominated by the BT component. The correlation values and regression slopes between the BT geostrophic and observed along-isobath currents are not significantly different than the values between the total geostrophic and observed along-isobath currents, indicating that the contribution of the BC geostrophic current to ST variability is small (see also Figure 12). The geostrophic and observed cross-isobath currents are less correlated than along-isobath flow, although the correlation values are still significant at the 99% confidence level (Figure 14). The vertical structure of the regression slopes between geostrophic and observed cross-isobath currents is similar to the along-isobath flow, with slopes greater than 1.0 near the surface (1.48 ± 0.62 at 4.6 m), smaller than 1.0 near the bottom (0.96 ± 0.23 at 67 m), and approximately 1.0 at mid-depths. However, the slopes are not significantly different from 1.0 near the surface and bottom. Below 30 m, the correlation between observed and total geostrophic cross-isobath current is substantially higher than the correlation between observed and BT geostrophic current, indicating that the contribution of the BC geostrophic current to the ST cross-isobath current variability is large.

[40] The structure exhibited by the linear regression slopes between the geostrophic and observed currents support the separation of the water column into distinct near-surface (0–20 m), interior (20–50 m), and (perhaps) near-bottom (0–20 mab) regions. The interior is highly geostrophic, while the surface and bottom regression slopes are significantly different from 1.0, particularly for the along-isobath flow. The evidence for a strongly ageostrophic bottom region is perhaps unclear. Regressions slopes between along-isobath currents departed slightly (but significantly) from 1.0 near the bottom, and there is no clear departure from geostrophy in the cross-isobath flow. Subtidal bottom stress variability is very small (about an order of magnitude less than wind stress) during CMO, suggesting that ageostrophic near-bottom currents are small as well and thus only a small departure from geostrophy in the regression slopes.

[41] The depth-averaged along-isobath geostrophic flow is most highly correlated (0.65) with the fluctuating wind stress component oriented 47°T and lagged the wind stress by 14 hours, similar to the observed depth-averaged along-isobath flow (Table 3). The comparison is nearly identical for the BT geostrophic flow (0.63, 49°T, 13 hours), while the along-isobath BC geostrophic currents (at any depth) are not significantly correlated with wind stress (in any direction). This strongly suggests that the geostrophic wind-driven response is barotropic and, given the substantial BC geostrophic flow on monthly and longer timescales, that the role of the BC geostrophic currents in the ST wind-driven response is to provide an essentially constant (on the timescale of the wind events) vertical structure (e.g., Figure 6) via thermal wind shear. The seasonal comparisons between wind stress and along-isobath geostrophic flow were nearly identical to the comparisons with the observed along-isobath flow (Table 3). The depth-averaged cross-isobath geostrophic flow was most highly correlated (0.29) with the wind stress component oriented 320°T and lagged the wind by 16 hours. The correlation was not statistically significant at the 99% level; however, the comparison was similar to the significant correlation, orientation, and lag seen in the observed cross-isobath flow (Table 3). During the fall and spring, wind stress and cross-isobath geostrophic flow were uncorrelated. During the winter, the maximum correlation was 0.38 for the wind stress oriented 311°T with a lag of 18 hours. The relationship between the depth-averaged observed and geostrophic cross-isobath currents and wind stress oriented roughly 330°T, while weak, hints at the possibility that the process of coastal setup/setdown may be at work along an alternate coastline. In this instance, Nantucket Shoals might serve as the "coast." Although the Nantucket Shoals are entirely submerged (minimum depth around 20 m), surface mixed layers are often deeper than 20 m, due to tidal mixing [*Limeburner and Beardsley*, 1982], making the setup/setdown process theoretically possible.

### 6.2. Subtidal Ageostrophic Current Variability

[42] Subtidal ageostrophic current variability is weaker in general than geostrophic current variability. Because BT geostrophic currents are required to estimate them, subtidal ageostrophic currents are band passed (33 hours to 65 days). Standard deviations for both the along- and cross-isobath ageostrophic flow range from about 2 to 7 cm $s^{-1}$. Ageostrophic current variability is strongest near surface, weakest at 54.5 m (about 15 mab), and increases slightly toward the bottom. Ageostrophic current variability is moderately polarized, and ellipticity of the ageostrophic ST current principal axes are between 0.6 and 0.8 (decreasing toward bottom), with an approximately cross-isobath orientation.

[43] Above 30 m, ageostrophic currents are correlated with wind stress. The maximum vector correlation between wind stress and ageostrophic currents at 4.6 m is 0.72, with an angle of 62° CW relative to the wind stress vector and a lag of zero hours. At 30 m, maximum vector correlation is 0.34 with an angle of 102° CW and a lag of zero hours. Relative angle between wind stress and currents turns CW

with depth consistent with Ekman dynamics. Below 30 m, ageostrophic currents are not significantly correlated with wind stress. Ageostrophic currents near the bottom are correlated with bottom stress. The maximum vector correlation between bottom stress and ageostrophic currents at 67 m (3 mab) is 0.54, with an angle of 113° CCW relative to the bottom stress vector and a lag of zero hours. At 59.5 m (10.5 mab), the maximum vector correlation between bottom stress and ageostrophic currents is 0.47, with an angle of 86° CCW relative to the bottom stress vector and a lag of zero hours. The relative angle between bottom stress and near bottom currents turns CW with height consistent with Ekman dynamics.

[44] Depth-averaged ageostrophic transport is comparable to total Ekman transport (scaled by depth) from equation (8). The depth-averaged along-isobath ageostrophic and Ekman transports have a correlation of 0.55 and linear regression slope of 0.68 ± 0.13, while cross-isobath transports have a correlation of 0.46 and smaller regression slope of 0.45 ± 0.12. Because ST along-isobath current variability is large and rapid accelerations of the along-isobath flow accompany most of the wind events (Figure 3), acceleration terms in the along-isobath momentum balance may contribute to the cross-isobath ageostrophic transport. Including the acceleration of the depth-averaged along-isobath flow ($\langle u_t \rangle$) by adding it to the Ekman transport does not change the correlation much (0.43) and increases the linear regression slope to 0.60 ± 0.17, suggesting that acceleration terms are significant in the ST along-isobath momentum balance. Including depth averages of the nonlinear along-isobath momentum terms ($\langle uu_x \rangle$ and $\langle vu_y \rangle$) did not significantly change the correlation or regression.

[45] Ageostrophic transport over the depth range 0–25 m is very similar to the purely wind-driven Ekman transport, computed from equation (8) with $\tau^b = 0$ and $H = 25$ m, with correlations of 0.74 and 0.61 and regression slopes of 1.19 ± 0.13 and 1.00 ± 0.17 for the along- and cross-isobath transports, respectively (Figure 15). Ageostrophic transport near the bottom (0–20 mab), although correlated, does not compare closely with Ekman transport estimated from bottom stress. Correlations between ageostrophic and Ekman transport between 20 mab and the bottom are 0.46 (along-isobath) and 0.51 (cross-isobath), and linear regression slopes are small, 0.19 ± 0.05 (along-isobath) and 0.34 ± 0.08 (cross-isobath). It is unknown what causes this large discrepancy in near-bottom ageostrophic transport.

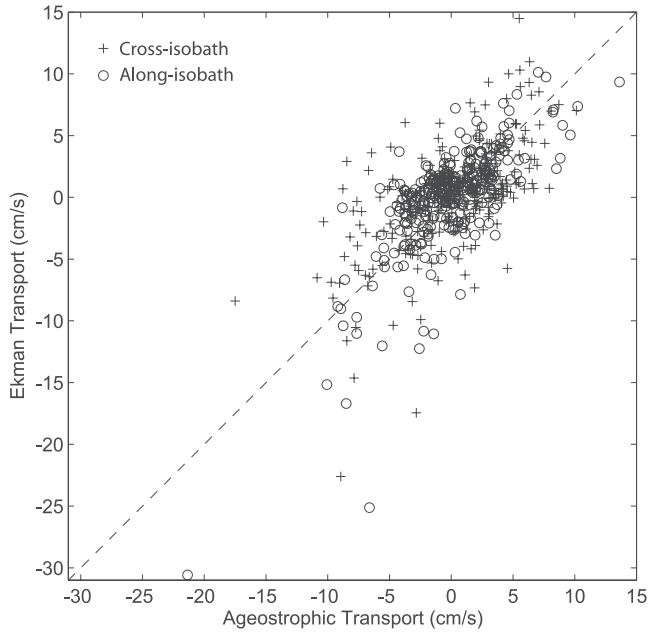


**Figure 15.** Subtidal depth-averaged ageostrophic current between 0 and 25 m and wind-driven Ekman transport scaled by 25 m.

## 7. Discussion

### 7.1. Coastline Orientation

[46] During CMO, the relationships between along-isobath currents and wind forcing depart from the simplest models of wind-driven setup/setdown [e.g., *Allen*, 1980; *Winant*, 1980] in that the along-isobath currents respond most strongly to the fluctuating wind stress component oriented 45°T, more cross-isobath than along-isobath. A similar coherence with a cross-isobath wind stress component (77°T) is noted by *Beardsley et al.* [1985], who conclude that 77°T corresponds to the orientation of the greater New England coastline, since the wind stress component parallel to the coast on relatively large length scales is most effective at driving along-isobath flow [*Allen*, 1980]. This raises two questions: What defines large length scales and what is an objective estimate of coastal orientation at these scales?

[47] According to *Pedlosky* [1974], subtidal along-shelf flow is most effectively driven by the along-coast wind stress component, where the length scale for determining the along-coast orientation is set by the wind-forcing. This scale is defined by a minimum critical length,

$$L_\theta = \frac{UH}{\tau^{scx}/\rho_0 f} L^y, \tag{9}$$

where $U$ is a characteristic along-shelf velocity, $H$ is the water depth, $L^y$ is the shelf width, and $\tau^{scx}/\rho_0 f$ is the Ekman transport due to a characteristic along-coast wind stress. The length $L_\theta$ represents the along-coast length scale over which the cross-shelf Ekman volume flux matches the along-shelf volume flux, suggesting that this is the scale at which these terms have equal dynamic importance. Choosing values applicable to the New England shelf from the CMO data ($U = 30$ cm s$^{-1}$, $H = 70$ m, $L^y = 100$ km, $\tau^{sx} = 0.2$ N m$^{-2}$) gives an $L_\theta$ of about 1000 km. This is comparable to the characteristic length scale of storms, 500–1500 km [*Beardsley and Haidvogel*, 1981], which are the primary source of strong ST wind stress variability and ST wind-driven flow on the New England shelf.

[48] The orientation of the wind stress component most effective at driving along-isobath flow on the New England shelf should match the coastline orientation on length scales of $L_\theta$ (1000 km) or more. To determine coastline orientation as a function of scale, a line is fit to the $x$,$y$ locations of high-resolution coastline data over 100- to 2000-km-long segments centered on the CMO site (Figure 16). Below a scale of 600 km, the average coastline orientation is highly variable and ranges from about 60 to 110°T, but for length

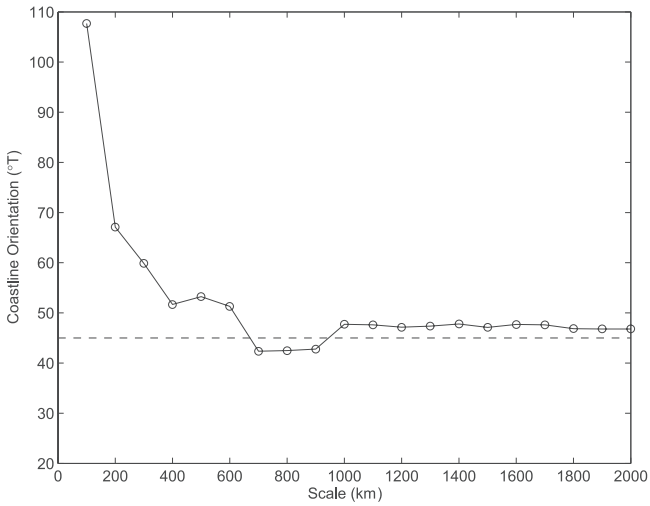


**Figure 16.** Estimates of coastline orientation from linear fit. Orientation is determined by the slope of the line, and scale is the approximate length of coastline (centered on the CMO site) used in the fit.

scales larger than 1000 km, the average coastline orientation is nearly constant at 47–48°T, matching closely with the observed orientation of the wind stress component that yields maximum correlation with the along-isobath flow (Table 3).

[49] *Pedlosky*'s [1974] hypothesis that length scale of the dominant wind forcing ($L_\theta$) determines the relevant coastline scale appears to explain the observed relationship between wind stress and depth-averaged currents during CMO. Passing storms with length scales of approximately 1000 km are the primary source of wind-driven currents on the New England shelf, and the coastline orientation on length scales of 1000 km (45°T) or more matches the orientation of the wind stress component most effective at driving subtidal along-isobath current fluctuations. The agreement is interesting considering the large coastline irregularity of the Gulf of Maine and the potential affects of propagating CTWs (not considered by Pedlosky). This supports the idea of a strongly local wind-driven response on the New England shelf.

[50] The orientation 45°T was originally cited by *Noble et al.* [1983] as the along-shelf orientation for the Mid-Atlantic Bight south of Nantucket Shoals, and 56°T was chosen as the along-shelf orientation for the modeling studies of *Wright et al.* [1986]. The wind stress orientation (77°T), identified as along-coast during NSFE, differs from the average coastline orientation, possibly because the comparison was not between wind stress and depth-averaged flow, but rather along-isobath flow at 32 m. Flow at 32 m depth is not necessarily below the directly wind-driven surface boundary layer, so correlations with wind stress will not only reflect the setup/setdown process, but also ageostrophic processes such as Ekman transport.

### 7.2. Forcing of Low-Frequency Current Variability

[51] What drives the low-frequency (timescales of months and longer) along-isobath flow on the New England shelf? The low-frequency flow is apparently not wind driven, at least not in a way that is consistent with the ST flow. The mean and seasonal mean wind stress generally oppose the mean along-isobath flow, and the intercepts of the linear regression analysis between along-coast wind stress and observed along-isobath currents (Figure 11d) are strikingly similar to the observed mean and seasonal mean currents (Figures 5a and 6a). The linear regression intercepts represent the currents that persist in the absence of wind forcing, and the similarity with the observed flow suggests that the low-frequency current fluctuations during CMO are not wind driven. This does not imply that there is zero mean wind-driven flow. Mean wind-driven flow is estimated as the mean along-coast wind stress multiplied by the linear regression slopes relating along-coast wind stress and along-isobath flow (Figure 11c). The depth-average of the mean wind-driven currents are less than 1 cm $s^{-1}$ over the full record. Low-frequency wind-driven flow is largest in winter, averaging about 2.5 cm $s^{-1}$, directed eastward along isobath. The downwelling-favorable events in fall result in a mean along-isobath flow of $-1.1$ cm $s^{-1}$, directed westward along isobath. The low-frequency wind-driven currents are very small compared to the observed currents.

[52] An along-shelf pressure gradient has been suggested as the driving mechanism for the low-frequency along-shelf flow in the MAB [*Stommel and Leetma*, 1972; *Csanady*, 1976]. Two sources for an along-shelf pressure gradient have been proposed; an on-shelf source, such as a localized upstream freshwater influx, creating an along-shelf pressure gradient through an along-shelf density gradient [*Chapman et al.*, 1986],or an off-shelf source, such as the gyre-scale pressure gradients, associated with large-scale wind stress, imposed as a boundary condition at the shelf break [*Csanady*, 1978; *Beardsley and Winant*, 1979]. During CMO, however, there are no significant correlations between the observed along-isobath pressure gradients and along-isobath currents on ST or monthly timescales (with the BT component for monthly values inferred as per section 5). Also, the seasonal mean cross-isobath geostrophic flow (representing the along-isobath pressure gradient) is the opposite sign necessary to drive westward along-isobath flow in these models.

[53] Furthermore, observations during CMO indicated that bottom stress (on both subtidal and low-frequency timescales) is very small. Mean and seasonal mean bottom stress is an order of magnitude smaller than the wind stress. This is significant, because bottom stress is an essential component of the models of low-frequency flows over the shelf [i.e., *Stommel and Leetma*, 1972; *Csanady*, 1976; *Chapman et al.*, 1986]. If bottom stress is indeed negligible, this significantly alters the dynamics of the flow. The small bottom stress observed during CMO may be a local anomaly. The CMO site is situated over a region with muddy sediments, as opposed to the more typical sandy or rocky sediments on the New England shelf. The muddy bottom may be less rough than sandy or rocky bottoms, and thus provide less stress. It is possible that bottom stress integrated over longer along-shelf length scales may be larger in magnitude, but further observations would be required to assess this possibility.

[54] An alternate model for the low-frequency along-isobath flow over the New England shelf is simply sheared geostrophic flow with zero current at the bottom boundary

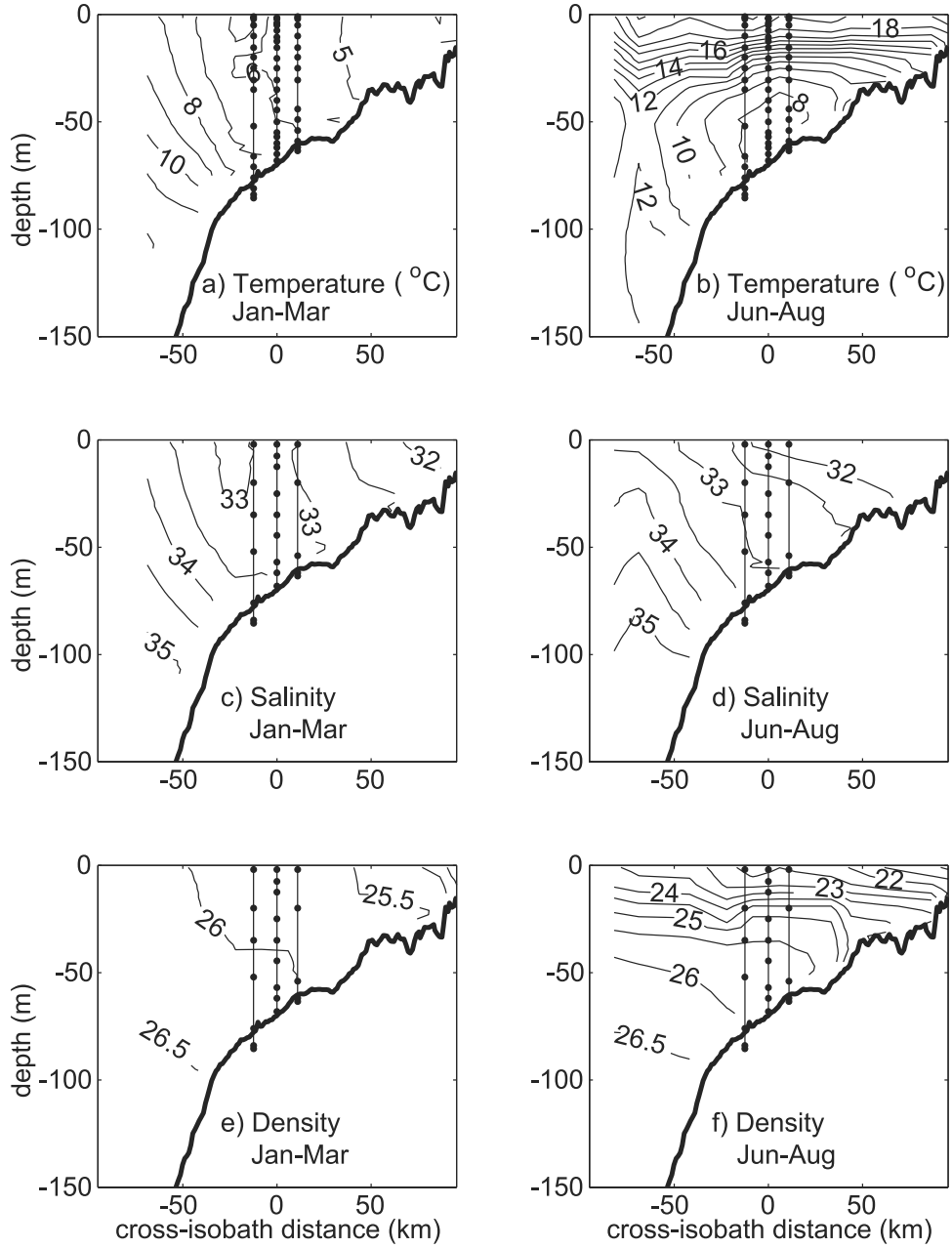


**Figure 17.** Average winter (January through March) and summer (June through August) cross-isobath sections of (a, b)temperature, (c, d) salinity, and (e, f) density, computed from historical NODC data on the New England shelf.

and fluctuations caused by changes in the cross-isobath density gradients, in particular, a strengthening of the cross-isobath density gradient and associated along-isobath geostrophic flow due to the seasonal changes in temperature on the New England shelf and the formation of the cold pool. Over the New England shelf, the cross-isobath structure of the low-frequency salinity field is relatively constant (there is some variability induced by local fresh water inputs) [*Lentz et al.*, 2003], transitioning from fresher inshore shelf water to saltier offshore slope water (Figure 17). However, the cross-isobath structure of the temperature field undergoes a large seasonal change (Figure 17). During the winter (and much of the spring) and in the shelf-slope front, the temperature gradient is negative, corresponding to cool water inshore and warm water offshore. During the summer, shallower inshore water warms and a cross-shelf temperature minimum forms, the cold pool. The temperature gradient changes sign from negative to positive inshore of the cold pool. The affect on the density field is to strengthen density gradients and enhance the along-isobath geostrophic flow inshore of the cold pool during the summer (Figure 18), because a positive temperature gradient augments the persistent, negative salinity gradient. This alternate model removes the need for along-shelf forcing by wind stress or pressure gradients. However, the alternate model does require some adjustment process to bring bottom currents

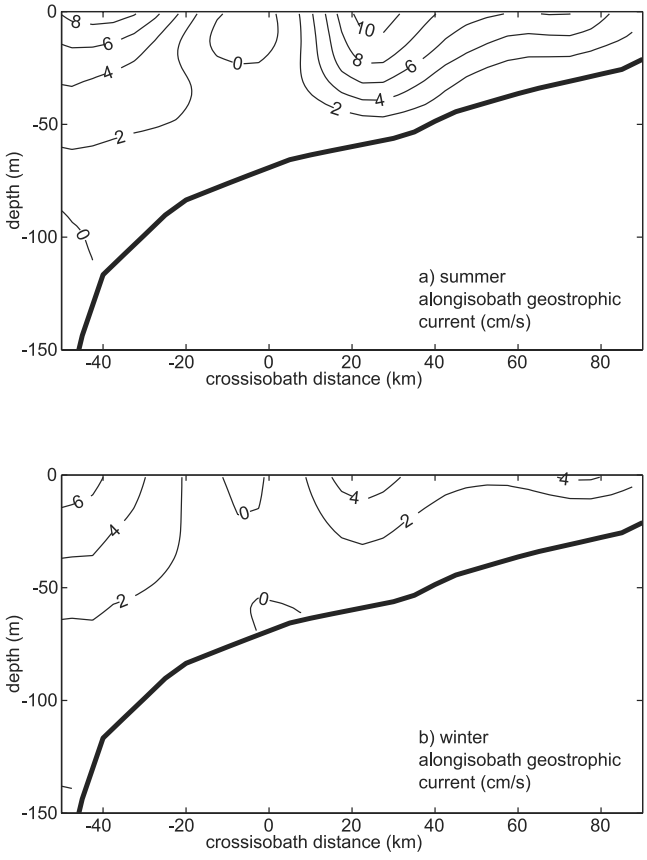


**Figure 18.** Along-isobath geostrophic flow (referenced to the bottom) computed from average (a) winter and (b) summer density sections.

back to zero as cross-isobath density gradients are changed. This might be accomplished through a process similar to the trapping of a coastal density front [e.g., *Chapman and Lentz*, 1994].

[55] During CMO, the contributions of temperature (T) and salinity (S) to the near bottom (0–20 mab) density gradient, and hence thermal wind shear via equation (7), are estimated using a linear relation,

$$\nabla\rho = \alpha\nabla T + \beta\nabla S, \tag{10}$$

where $\nabla$ is the horizontal gradient operator and $\alpha = -0.15$ and $\beta = 0.82$ (estimated by linear regression). The affect of monthly mean cross-isobath salinity gradients are always negative, corresponding to fresher water inshore, with a persistent mean value of about $-2.0 \times 10^{-5}$ kg m$^{-4}$ (Figure 19a). The cross-isobath temperature gradients have a similar range of variability with regard to their effect on density, but a near-zero mean value. During August through November, the temperature gradient is positive (warmer water inshore), resulting in a negative contribution to the total density gradient. During the fall, the cross-isobath temperature and salinity gradients act in concert to create the strongest cross-isobath density gradients during CMO. The cross-isobath temperature gradient changed sign in December through April, corresponding to cooler water inshore. The cross-isobath salinity gradients do peak during the winter, but the total density gradient remains constant, because the temperature gradient opposes the increasing salinity gradient. During the winter, the foot of the shelf-slope front is inshore of the central site [*Lentz et al.*, 2003]. Interestingly, the onshore position of the shelf-slope front in winter does not correspond to the strongest low-frequency cross-isobath density gradients. This is because temperature and salinity gradients oppose each other (partially compensate) in the shelf-slope front. This reinforces the importance of the cold pool and the seasonal heating cycle to the flow field on the New England shelf.

[56] The alternate model for low-frequency along-isobath flow is consistent with the CMO estimates of geostrophic flow, seasonally reversing cross-isobath temperature gradients, and very small bottom stress. By extending the BC geostrophic along-isobath currents to the bottom (constant shear), a monthly mean BT geostrophic flow is estimated, such that the total geostrophic flow is zero at the bottom. This geostrophic flow is similar to the low-frequency non-wind-driven flow, estimated as the intercepts from linear regression of the along-coast wind stress onto the depth-averaged along-isobath currents over monthly intervals (Figure 19b). The monthly estimates of non-wind-driven currents are highly correlated (0.79) with the depth-averaged geostrophic flow. There is a substantial offset of 2 ± 5 cm s$^{-1}$ (estimated by linear regression) between the depth-averaged geostrophic and non-wind-driven flow, which is due to the assumption that geostrophic flow is zero at the bottom when the observations suggest that flow at the bottom is about 3 cm s$^{-1}$ (Figure 5a). The alternate model does not preclude the driving of along-isobath flow by an along-shelf pressure gradient, and along-shelf pres-

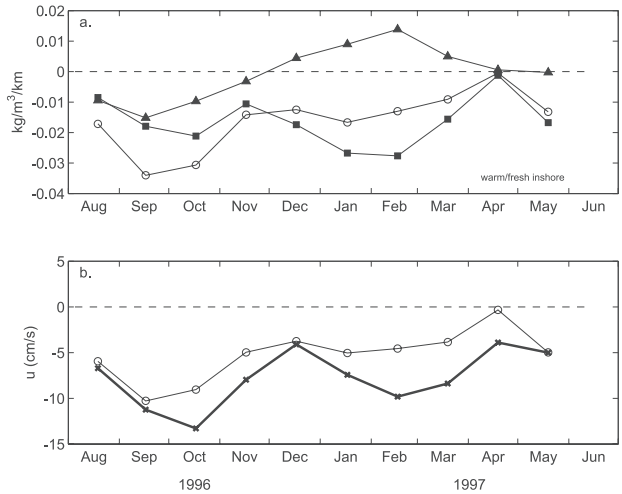


**Figure 19.** (a) Monthly mean near-bottom cross-isobath temperature (triangles) and salinity (squares) gradients, scaled to represent their contribution to the total density gradient (circles). A negative cross-isobath gradient indicates warmer/fresher water inshore. (b) Comparison of monthly estimates of along-isobath depth-averaged non-wind-driven flow (crosses) and the alternate model monthly mean BT (solid circles) and depth-averaged geostrophic (open circles) flow.

sure gradient driving could possibly explain the persistent 2 cm $s^{-1}$ difference.

## 8. Summary

[57] Velocity variability over the New England shelf on timescales from days to months has been described using observations from a moored array deployed from August 1996 to June 1997 as part of the Coastal Mixing and Optics program. The dominant terms in the horizontal momentum balances were determined using bottom pressure, density, surface stress, and bottom stress observations from the moored array. The characteristics and dynamics of current variability on timescales from days to weeks was different from the variability at timescales of months.

[58] The current variability on timescales of days to weeks (subtidal) was polarized along isobath and dominated by episodic bursts of westward flow (Figure 3). This along-isobath flow was primarily geostrophic and barotropic; that is, the Coriolis force associated with the along-isobath flow was largely balanced by a barotropic cross-isobath pressure gradient (Figures 12 and 13). This along-isobath geostrophic flow was correlated with the large-scale along-coast wind stress (orientation 45°T or 65° CCW from the local isobath) consistent with the process of coastal setup/setdown. The appropriate scale for defining the along-coast orientation (about 1000 km) is consistent with a scaling, equation (9), based on the ratio of the along-shelf transport to the cross-shelf Ekman transport [*Pedlosky*, 1974]. The wind-driven flow persists for longer in fall and spring (stratified periods) than in winter (unstratified) (Figure 10). The subtidal cross-isobath flow also has a substantial geostrophic component; however, the baroclinic is similar in magnitude to the barotropic components and of opposite sign (Figures 12 and 13). Depth-integrated Ekman transport, estimated from wind and bottom stress, accounted for a large fraction of the depth-averaged ageostrophic transport. The subtidal ageostrophic transport in the upper 25 m closely matched estimates of Ekman transport from wind stress; however, near-bottom ageostrophic transport was much larger than Ekman transport estimated from bottom stress. Measured bottom stress was nearly an order of magnitude smaller than the wind stress at subtidal timescales and a factor of 5 or more smaller than assumed in previous studies of the dynamics in this region [e.g., *Stommel and Leetma*, 1972; *Chapman et al.*, 1986].

[59] On monthly and longer timescales, currents were generally westward and off-shelf at all sites and depths, with the strongest westward flows during the fall (Figure 3). This along-isobath current was primarily geostrophic, but in contrast to the shorter timescale variability, the baroclinic component of the geostrophic flow was similar in magnitude to the barotropic component. In the along-isobath direction, the monthly mean ageostrophic flow was weak relative to the geostrophic flow, while in the cross-isobath direction the two were of similar magnitudes. Depth-averaged ageostrophic transport was consistent with Ekman transport from wind and bottom stress. Bottom stress at these timescales was weak, nearly an order of magnitude smaller than the wind stress. A key result of this study is that seasonal variations in the mean along-isobath current were attributable to variations in the cross-shelf density field associated with the seasonal cycle in surface heating/cooling. During the fall, thermal wind shear in the lower water column was strongest with the cross-isobath temperature gradient acting in concert with the relatively constant cross-isobath salinity gradients to enhance the cross-isobath density gradient (i.e., warmer and fresher water inshore). During the winter, in response to surface cooling, the cross-isobath temperature gradient reversed sign, reducing the cross-isobath density gradient (i.e., cooler water inshore).

## Appendix A: Estimating Geostrophic Velocity

[60] Absolute geostrophic velocity ($\mathbf{u}^g$) is estimated from the observations of density ($\rho$) and bottom pressure ($P^b$). Density was determined from conductivity and temperature measurements at several depths throughout the water column at the inshore (2, 20, 54, 61.9, 63.5 m), central (2, 7.5, 12.5, 25, 35, 44.5, 57, 62, 68.1 m), offshore (2, 20, 35, 52, 76, 83.9, 85.5 m), and alongshore (2, 20, 40, 60, 67.9, 69.5 m) sites. The return on density observations was 88% (7381 data days out of 8370 possible data days). At each site, gaps were filled using linear interpolation (in the vertical), when density data existed above and below the gap. At the central site, the shallowest conductivity observation (2 m) ceased logging data on 3 September 1996 (coincident with the passage of Hurricane Edouard). Since no density data exist above 2 m at the central site, vertical interpolation was not possible. Therefore a linear relationship between temperature and sigma-t was estimated (least squares) using colocated data from the central site at each hourly interval. The temperature observation at 2 m and the linear temperature and sigma-t relation were then used to fill the remainder of the time series. As a test, the linear temperature and sigma-t relation was applied to the temperature time series at 7.5 m and compared to the actual sigma-t time series at that depth. The result was a correlation of 0.998, a linear regression slope of 0.995, and an rms difference of 0.05 (sigma-t units). Temporal gaps remain in the upper water column data at the inshore and alongshore sites during periods when the respective surface moorings had broken loose.

[61] There were no temporal gaps in the bottom pressure data; however, no observation was made at the central site. Bottom pressure at the central site and bottom pressure gradients were estimated by using a plane to represent the horizontal variability,

$$P^b(x,y,t) = m(t)x + n(t)y + c(t), \tag{A1}$$

where again $x$ and $y$ are the along- and cross-isobath coordinates (with $x_c$, $y_c$ = 0, 0), $m = \partial P^b/\partial x$ and $n = \partial P^b/\partial y$ are the along- and cross-isobath bottom pressure gradients, and $c$ is the bottom pressure at the central site ($P^b_c$). The linear system of equations created from equation (A1) by $P^b_i$, $P^b_o$ and $P^b_a$ was solved for $m$, $n$, and $c$ using Gaussian elimination.

[62] Bottom pressure measurements are vulnerable to relative large amplitude, low-frequency noise with timescales of weeks to months or longer [*Brown et al.*, 1987; *Harms and Winant*, 1994]. With respect to the calculation of gradients, the linear trends and mean values of bottom pressure time series are typically discarded as unreliable [*Brown et al.*, 1985]. Linear trends were identified and

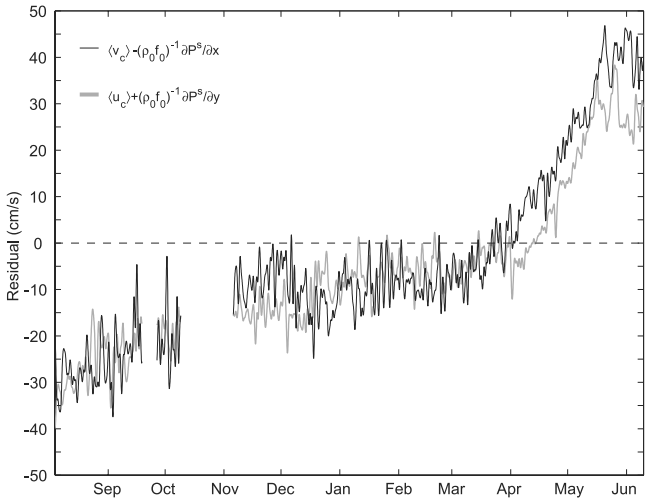


**Figure A1.** Residual between depth-averaged and geostrophic currents estimated from the gradients of pressure at $z = 0$, computed via equation (3). Bottom pressure records at the offshore and alongshore sites have had a mean and linear trend removed, while bottom pressure at the inshore site has only had a mean removed.

removed from the bottom pressure observations at the offshore (0.8 mbar month$^{-1}$) and alongshore (1.7 mbar month$^{-1}$) sites. Bottom pressure at the inshore site, however, contained a low-frequency error component not adequately explained by a simple linear drift. As a check, the bottom pressure gradient was computed via equation (A1), using the detrended observations of $P_o{}^b$ and $P_a{}^b$ and the unmodified observations of $P_i{}^b$, and compared to the pressure gradient required to geostrophically balance the depth-averaged flow at the central site. It is assumed that the remaining large amplitude, low-frequency noise is attributable to the inshore observation, and that the depth-averaged, geostrophic estimate is similar enough to the actual bottom pressure gradient to reveal any large amplitude, low-frequency noise in the difference with the observed bottom pressure gradient. The low-frequency component of the residual bottom pressure gradient is nearly identical for both the along- and cross-isobath gradients (Figure A1). The negative along-isobath bottom pressure gradient residual is shown to keep the sense of any error at the inshore site positive. The similarity in both residuals supports the assumption that remaining low-frequency noise comes from the inshore bottom pressure observation. The residual suggests a drift-like low-frequency noise at the inshore site from August to November 1996, then a period of no drift, followed by a more rapid drift from April to June. Irregular, gradual sinking of the anchor on which the inshore bottom pressure gauge was mounted could explain this low-frequency signal. There is no objective means for removing this low-frequency noise. Therefore, to remove the low-frequency noise component, any estimates that require bottom pressure gradients are band-pass filtered to exclude variability at timescales longer than 65 days.

[63] Pressure at $z = 0$ is computed from the observations of bottom pressure and density, using equation (3). Pressure throughout the water column is computed $P = P^0 + B$, where the baroclinic pressure ($B$) is computed from equation (4). The integrals in equations (3) and (4) are evaluated by trapezoidal integration, using the discrete observation points at each site. Geostrophic velocity is separated into BT and BC components, and computed from equations (5) and (6). Depth-dependent pressure gradients are computed using a sigma-coordinate ($z/h$) in the vertical. The profiles of $B$ at the different sites ($B_i$, $B_c$, $B_o$, $B_a$) are linearly interpolated to the sigma-levels that match the current observations at the central site. Gradients of $B$ are estimated by fitting (least squares) a plane to the four observations at each sigma-level.

[64] For comparison with the geostrophic currents, VMCM observations are spatially averaged, following *Brown et al.* [1985],

$$u^{obs} = \frac{1}{\Delta y}\int_{y_o}^{y_i} u\,dy \tag{A2}$$

$$v^{obs} = \frac{1}{\Delta x}\int_{x_c}^{x_a} v\,dx, \tag{A3}$$

where $\Delta x$ = 14.5 km and $\Delta y$ = 23.3 km are the along-isobath (alongshore to central) and cross-isobath (inshore to offshore) mooring separations. Observed currents are interpolated to the same depths as the geostrophic current estimates. Results do not change qualitatively using only VMCM observations at the central site.

[65] **Acknowledgments.** The design, deployment, and recovery of the moored array, the preparation of the instruments, and processing of the data were done by N. Galbraith, W. Ostrom, R. Payne, R. Trask, G. Tupper, J. Ware, and B. Way of the Upper Ocean Processes Group at WHOI with assistance from M. Baumgartner, C. Marquette, Lt. M. Martin, N. McPhee, E. Terray, and S. Worrilow. The moorings were fabricated by the WHOI Rigging Shop under the direction of D. Simoneau. Funding was provided by the Office of Naval Research, Code 322, under grant N00014-95-1-0339. R. K. S. thanks the Postdoctoral Scholar Program at the Woods Hole Oceanographic Institution, with funding provided by the Devonshire Foundation.

## References

Aikman, F., III, H. W. Ou, and R. W. Houghton, Current variability across the New England continental shelf-break and slope, *Cont. Shelf Res.*, *8*, 625–651, 1988.

Allen, J. S., Models of wind-driven currents on the continental shelf, *Annu. Rev. Fluid Mech.*, *12*, 389–433, 1980.

Beardsley, R. C., A comparison of the vector-averaging current meter and New Edgerton, Germeshausen, and Grier, Inc., vector-measuring current meter on a surface mooring in Coastal Ocean Dynamics Experiment 1, *J. Geophys. Res.*, *92*, 1845–1860, 1987.

Beardsley, R. C., and D. B. Haidvogel, Model studies of the wind-driven transient circulation in the Middle Atlantic Bight: 1. Adiabatic boundary conditions, *J. Phys. Oceanogr.*, *11*, 355–375, 1981.

Beardsley, R. C., and C. D. Winant, On the mean circulation in the Mid-Atlantic Bight, *J. Phys. Oceanogr.*, *9*, 612–619, 1979.

Beardsley, R. C., D. C. Chapman, K. H. Brink, S. R. Ramp, and R. Schlitz, The Nantucket Shoals Flux Experiment (NSFE79): I. A basic description of the current and temperature variability, *J. Phys. Oceanogr.*, *15*, 713–748, 1985.

Bigelow, H. B., Studies of the waters on the continental shelf, Cape Cod to Chesapeake Bay: I. The cycle of temperature, *Pap. Phys. Oceanogr. Meteorol.*, *2*, 1–135, 1933.

Brown, W. S., N. R. Pettigrew, and J. D. Irish, The Nantucket Shoals Flux Experiment (NSFE79): II: The structure and variability of across-shelf pressure gradients, *J. Phys. Oceanogr.*, *15*, 749–771, 1985.

Brown, W. S., J. D. Irish, and C. D. Winant, A description of subtidal pressure field observations on the northern California continental shelf during the Coastal Ocean Dynamics Experiment, *J. Geophys. Res.*, *92*, 1605–1635, 1987.

Chang, G. C., and T. D. Dickey, Optical and physical variability on timescales from minutes to the seasonal cycle on the New England Shelf: July 1996–June 1997, *J. Geophys. Res.*, *106*, 9435–9453, 2001.

Chapman, D. C., and S. J. Lentz, Trapping of a coastal density front by the bottom boundary layer, *J. Phys. Oceanogr.*, *24*, 1464–1479, 1994.

Chapman, D. C., J. A. Barth, R. C. Beardsley, and R. G. Fairbanks, On the continuity of mean flow between the Scotian Shelf and the Middle Atlantic Bight, *J. Phys. Oceanogr.*, *16*, 758–772, 1986.

Csanady, G. T., Mean circulation in shallow seas, *J. Geophys. Res.*, *81*, 5389–5399, 1976.

Csanady, G. T., The arrested topographic wave, *J. Phys. Oceanogr.*, *8*, 47–62, 1978.

Dickey, T. D., and A. J. Williams III, Interdisciplinary ocean process studies on the New England shelf, *J. Geophys. Res.*, *106*, 9427–9434, 2001.

Edson, J. B., A. A. Hinton, K. E. Prada, J. E. Hare, and C. W. Fairall, Direct covariance flux estimates from mobile platforms at sea, *J. Atmos. Oceanic Technol.*, *15*, 547–562, 1999.

Fairall, C. W., E. F. Bradley, D. P. Rogers, J. B. Edson, and G. S. Young, Bulk parameterization of air-sea fluxes for Tropical Ocean-Global Atmosphere Coupled-Ocean Atmosphere Response Experiment, *J. Geophys. Res.*, *101*, 3747–3764, 1996.

Galbraith, N., A. Plueddemann, S. Lentz, S. Anderson, M. Baumgartner, and J. Edson, Coastal Mixing and Optics experiment moored array data report, *Tech. Rept. WHOI-99-15*, Woods Hole Oceanogr. Inst., Woods Hole, Mass., 1999.

Garrett, C., P. MacCready, and P. Rhines, Boundary mixing and arrested Ekman layers: Rotating stratified flow near a sloping boundary, *Annu. Rev. Fluid Mech.*, *25*, 291–323, 1993.

Greenberg, D. A., J. W. Loder, Y. Shen, D. R. Lynch, and C. E. Naimie, Spatial and temporal structure of the barotropic response of the Scotian Shelf and Gulf of Maine to surface wind stress: A model-based study, *J. Geophys. Res.*, *102*, 20,897–20,915, 1997.

Harms, S., and C. D. Winant, Synthetic subsurface pressure derived from bottom pressure and tide gauge observations, *J. Atmos. Oceanic Technol.*, *11*, 1625–1637, 1994.

Houghton, R. W., R. Schlitz, R. C. Beardsley, B. Butman, and J. L. Chamberlin, The Middle Atlantic Bight cold pool: Evolution of the temperature structure during summer 1979, *J. Phys. Oceanogr.*, *12*, 1019–1029, 1982.

Houghton, R. W., F. Aikman III, and H. W. Ou, Shelf-slope frontal structure and cross-shelf exchange at the New England shelf-break, *Cont. Shelf Res.*, *8*, 687–710, 1988.

Islen, C. O., A study of the circulation of the western North Atlantic, *Pap. Phys. Oceanogr. Meteorol.*, *2*, 1–101, 1936.

Kunze, E., Near-inertial wave propagation in geostrophic shear, *J. Phys. Oceanogr.*, *15*, 544–565, 1985.

Lentz, S., K. Shearman, S. Anderson, A. Plueddemann, and J. Edson, Evolution of stratification over the New England shelf during the Coastal Mixing and Optics study, August 1996–June 1997, *J. Geophys. Res.*, *108*(C1), 3008, doi:10.1029/2001JC001121, 2003.

Limeburner, R., and R. C. Beardsley, The seasonal hydrography and circulation over Nantucket Shoals, *J. Mar. Res.*, *40*, 371–406, 1982.

Linder, C. A., and G. Gawarkiewicz, A climatology of the shelfbreak front in the Middle Atlantic Bight, *J. Geophys. Res.*, *103*, 18,405–18,423, 1998.

Martin, M. J., An investigation of momentum exchange parameterizations and atmospheric forcing for the Coastal Mixing and Optics program, Master's thesis, Mass. Inst. of Technol./Woods Hole Oceanogr. Inst., Woods Hole, Mass., 1998.

Noble, M., B. Butman, and E. Williams, On the longshelf structure and dynamics of subtidal currents on the eastern United States continental shelf, *J. Phys. Oceanogr.*, *13*, 2125–2147, 1983.

Ou, H. W., R. C. Beardsley, D. Mayer, W. C. Boicourt, and B. Butman, An analysis of subtidal current fluctuations in the Middle Atlantic Bight, *J. Phys. Oceanogr.*, *11*, 1383–1392, 1981.

Pedlosky, J., On coastal jets and upwelling in bounded basins, *J. Phys. Oceanogr.*, *4*, 3–18, 1974.

Schwing, F. B., et al., Subtidal response of Scotian Shelf circulation to local and remote forcing: I. Observations, *J. Phys. Oceanogr.*, *22*, 523–541, 1992a.

Schwing, F. B., Subtidal response of Scotian Shelf circulation to local and remote forcing: II. Barotropic model, *J. Phys. Oceanogr.*, *22*, 542–563, 1992b.

Shaw, W. J., J. H. Trowbridge, and A. J. Williams III, The budget of turbulent kinetic energy and scalar variance in the continental shelf bottom boundary layer, *J. Geophys. Res.*, *106*, 9551–9564, 2001.

Stommel, H., and A. Leetma, Circulation on the continental shelf, *Proc. Natl. Acad. Sci., U.S.*, *69*, 3380–3384, 1972.

Wang, D. P., Low-frequency sea level variability on the Middle Atlantic Bight, *J. Mar. Res.*, *37*, 683–697, 1979.

Williams, A. J., III, J. S. Tochko, R. L. Koehler, W. D. Grant, T. F. Gross, and C. V. R. Dunn, Measurement of turbulence in the oceanic bottom boundary layer with an acoustic current meter array, *J. Atmos. Oceanic Technol.*, *4*, 312–327, 1987.

Winant, C. D., Coastal circulation and wind-induced currents, *Annu. Rev. Fluid Mech.*, *12*, 271–301, 1980.

Wright, D. G., D. A. Greenberg, J. W. Loder, and P. C. Smith, The steady-state barotropic response of the Gulf of Maine and adjacent regions to surface wind stress, *J. Phys. Oceanogr.*, *16*, 947–966, 1986.

S. J. Lentz and R. K. Shearman, Department of Physical Oceanography, Woods Hole Oceanographic Institution, Woods Hole, MA 02543, USA. (slentz@whoi.edu; rshearman@whoi.edu)